Phenomenology of high-ozone episodes in NE Spain

Querol, Xavier; Gangoiti, Gotzon; Mantilla, Enrique; Alastuey, Andrés; Minguillón, Maria Cruz; Amato, Fulvio; Reche, Cristina; Viana, Mar; Moreno, Teresa; Karanasiou, Angeliki; Rivas, Ioar; Pérez, Noemí; Ripoll, Anna; Brines, Mariola; Ealo, Marina; Pandolfi, Marco; Lee, Hong Ku; Eun, Hee Ram; Park, Yong Hee; Escudero, Miguel

DOI:
10.5194/acp-17-2817-2017

Document Version
Publisher's PDF, also known as Version of record

Citation for published version (Harvard):
Querol, X, Gangoiti, G, Mantilla, E, Alastuey, A, Minguillón, MC, Amato, F, Reche, C, Viana, M, Moreno, T, Karanasiou, A, Rivas, I, Pérez, N, Ripoll, A, Brines, M, Ealo, M, Pandolfi, M, Lee, HK, Eun, HR, Park, YH, Escudero, M, Beddows, D, Harrison, RM, Bertrand, A, Marchand, N, Lyasota, A, Codina, B, Olid, M, Udina, M, Jiménez-Esteve, B, Jiménez-Esteve, BB, Alonso, L, Millán, M & Ahn, KH 2017, 'Phenomenology of high-ozone episodes in NE Spain', *Atmospheric Chemistry and Physics*, vol. 17, no. 4, pp. 2817-2838. https://doi.org/10.5194/acp-17-2817-2017

Atmos. Chem. Phys., 17, 2817–2838, 2017
www.atmos-chem-phys.net/17/2817/2017/
doi:10.5194/acp-17-2817-2017

Atmospheric Chemistry and Physics Open Access EGU

Phenomenology of high-ozone episodes in NE Spain

Xavier Querol[1], Gotzon Gangoiti[2], Enrique Mantilla[3], Andrés Alastuey[1], Maria Cruz Minguillón[1], Fulvio Amato[1], Cristina Reche[1], Mar Viana[1], Teresa Moreno[1], Angeliki Karanasiou[1], Ioar Rivas[1], Noemí Pérez[1], Anna Ripoll[1], Mariola Brines[1], Marina Ealo[1], Marco Pandolfi[1], Hong-Ku Lee[4], Hee-Ram Eun[4], Yong-Hee Park[4], Miguel Escudero[5], David Beddows[6], Roy M. Harrison[6,a], Amelie Bertrand[7], Nicolas Marchand[7], Andrei Lyasota[8,†], Bernat Codina[8], Miriam Olid[8], Mireia Udina[8], Bernat Jiménez-Esteve[8], María R. Soler[8], Lucio Alonso[2], Millán Millán[3], and Kang-Ho Ahn[4]

[1]Institute of Environmental Assessment and Water Research, IDAEA-CSIC, C/Jordi Girona 18–26, 08034 Barcelona, Spain
[2]Escuela Técnica Superior Ingeniería de Bilbao, Departamento Ingeniería Química y del Medio Ambiente, Universidad del País Vasco UPV/EHU, Urkixo Zumarkalea, S/N, 48013 Bilbao, Spain
[3]Centro de Estudios Ambientales del Mediterráneo, CEAM, Unidad Asociada al CSIC, Parque Tecnológico C/Charles R. Darwin, 14 46980 Paterna, Valencia, Spain
[4]Department of Mechanical Engineering, Hanyang University, Ansan 425-791, Republic of Korea
[5]Centro Universitario de la Defensa de Zaragoza, Academia General Militar, Ctra. de Huesca s/n, 50090 Zaragoza, Spain
[6]Division of Environmental Health & Risk Management, School of Geography, Earth & Environmental Sciences, University of Birmingham, Edgbaston, Birmingham B15 2TT, UK
[7]Aix Marseille Univ, CNRS, LCE, 13331 Marseille, France
[8]Department of Astronomy and Meteorology, Faculty of Physics, University of Barcelona, Martí I Franquès 1, 08028 Barcelona, Spain
[a]also at: Department of Environmental Sciences/Centre for Excellence in Environmental Studies, King Abdulaziz University, Jeddah, Saudi Arabia
[†]deceased

Correspondence to: Xavier Querol (xavier.querol@idaea.csic.es) and Kang-Ho Ahn (khahn@hanyang.ac.kr)

Received: 14 October 2016 – Discussion started: 10 November 2016
Revised: 17 January 2017 – Accepted: 23 January 2017 – Published: 23 February 2017

Abstract. Ground-level and vertical measurements (performed using tethered and non-tethered balloons), coupled with modelling, of ozone (O_3), other gaseous pollutants (NO, NO_2, CO, SO_2) and aerosols were carried out in the plains (Vic Plain) and valleys of the northern region of the Barcelona metropolitan area (BMA) in July 2015, an area typically recording the highest O_3 episodes in Spain. Our results suggest that these very high O_3 episodes were originated by three main contributions: (i) the surface fumigation from high O_3 reservoir layers located at 1500–3000 m a.g.l. (according to modelling and non-tethered balloon measurements), and originated during the previous day(s) injections of polluted air masses at high altitude; (ii) local/regional photochemical production and transport (at lower heights) from the BMA and the surrounding coastal settlements, into the inland valleys; and (iii) external (to the study area) contributions of both O_3 and precursors. These processes gave rise to maximal O_3 levels in the inland plains and valleys northwards from the BMA when compared to the higher mountain sites. Thus, a maximum O_3 concentration was observed within the lower tropospheric layer, characterised by an upward increase of O_3 and black carbon (BC) up to around 100–200 m a.g.l. (reaching up to 300 µg m^{-3} of O_3 as a 10 s average), followed by a decrease of both pollutants at higher altitudes, where BC and O_3 concentrations alternate in layers with parallel variations, probably as a consequence of the atmospheric transport from the BMA and the return flows (to the sea) of strata injected at certain heights the previous day(s). At the highest altitudes reached in this study with the tethered balloons (900–1000 m a.g.l.) during the campaign, BC and O_3 were often anti-correlated or unrelated, possibly due to a prevailing regional or even hemispheric contribution

of O_3 at those altitudes. In the central hours of the days a homogeneous O_3 distribution was evidenced for the lowest 1 km of the atmosphere, although probably important variations could be expected at higher levels, where the high O_3 return strata are injected according to the modelling results and non-tethered balloon data.

Relatively low concentrations of ultrafine particles (UFPs) were found during the study, and nucleation episodes were only detected in the boundary layer.

Two types of O_3 episodes were identified: type A with major exceedances of the O_3 information threshold ($180\,\mu g\,m^{-3}$ on an hourly basis) caused by a clear daily concatenation of local/regional production with accumulation (at upper levels), fumigation and direct transport from the BMA (closed circulation); and type B with regional O_3 production without major recirculation (or fumigation) of the polluted BMA/regional air masses (open circulation), and relatively lower O_3 levels, but still exceeding the 8 h averaged health target.

To implement potential O_3 control and abatement strategies two major key tasks are proposed: (i) meteorological forecasting, from June to August, to predict recirculation episodes so that NO_x and VOC abatement measures can be applied before these episodes start; (ii) sensitivity analysis with high-resolution modelling to evaluate the effectiveness of these potential abatement measures of precursors for O_3 reduction.

1 Introduction

Ozone (O_3) is an airborne secondary pollutant that is produced through the photo oxidation of volatile organic compounds (VOCs) in the presence of nitrogen oxides ($NO_x = NO + NO_2$), with more intensive production in high insolation regions. It is well known that its formation processes are very complex and that the reaction and production rates are not linear (Monks et al., 2015, and references therein). According to EEA (2015), 97 % of the European population is exposed to O_3 concentrations that exceed the WHO guideline (see below) for the protection of human health. The complexity of this pollutant is also reflected in its air quality targets; thus, the European air quality directive 2008/50/EC establishes a number of O_3 target values (which are not legally binding, as opposed to the limit values set for the majority of pollutants):

- A human health target value fixed at $120\,\mu g\,m^{-3}$ as 8 h maximum in a day that should not be exceeded more than 25 days in a year as a 3-year mean. This target value was (arbitrarily) increased from the recommended $100\,\mu g\,m^{-3}$ in the WHO air quality guidelines (where no specific number of exceedances is recommended).
- A population information hourly threshold of $180\,\mu g\,m^{-3}$.
- A population alert hourly threshold of $240\,\mu g\,m^{-3}$.
- A vegetation protection target, AOT40 (expressed in $\mu g\,m^{-3}$ h), as the sum of the excess of hourly concentrations above $80\,\mu g\,m^{-3}$ in a given period using hourly values measured between 08:00 and 20:00, Central Europe Time (CET), for every day. Hourly AOT40 from May to July should not exceed $18\,000\,\mu g\,m^{-3}$ h O_3 as a 5-year mean.

NO_x has a catalytic effect in O_3 generation, and is only removed from the system by either deposition or oxidation to nitric acid (HNO_3) and reaction with VOCs to yield secondary aerosols, such as inorganic and organic nitrates, which may sequester a significant fraction of NO_x. Consequently, O_3 generation involves not only local and regional air masses but also long-range transport. Thus, as a general observation, long-range transport of O_3 and its precursors influence markedly the background O_3 levels in Europe (UNECE, 2010; Doherty et al., 2013). However, this situation might be very different when considering the high summer O_3 episodes of southern Europe (e.g. Millán et al., 1997, 2000; Palacios et al., 2002; Castell et al., 2008a, b, 2012; Stein et al., 2005; Escudero et al., 2014; Pay et al., 2014; Querol et al., 2016).

In the western Mediterranean Basin the problem of tropospheric O_3 has been intensively studied since the early 1980s (Millán et al., 1991, 1996a, b, c, 2000, 2002; Millán, 2002; Millán and Sanz, 1999; Mantilla et al., 1997; Salvador et al., 1997, 1999; Gangoiti et al., 2001; Stein et al., 2004, 2005; Dieguez et al., 2009, 2014; Doval et al., 2012; Castell et al., 2008a, b, 2012; Escudero et al., 2014). Results have evidenced that (i) the meteorology driving O_3 fluctuation in this region is markedly influenced by a very complex orography, with high mountain chains surrounding the basin; (ii) in summer, the lack of a marked synoptic advection caused by the presence of the Azores anticyclone and the Iberian and North African thermal lows, together with the sea and land breezes, give rise to air mass recirculation episodes (lasting for several days); and (iii) during these summer vertical and horizontal recirculations of air masses loaded with O_3 precursors and coinciding with high insolation and elevated biogenic VOCs (BVOCs) emissions (Seco et al., 2011), high O_3 concentrations may be recorded.

Millán's team results demonstrated that western Mediterranean Basin dynamics are very different from those in central Europe. The latter are dominated by neutral-cloudy conditions, where O_3 episodes are usually associated with advection, and transformation takes place within large displacements of air masses. There, morning fumigation from a high O_3 residual (and stratified) boundary layer (BL) formed over the previous days, in addition to local formation in the sunny midday period may give rise to peak O_3 episodes if conditions persist after several days. In contrast, vertical recirculations developed over all western Mediterranean coastal areas, determine a very different O_3 dynamics. Air masses travel all

the way from the sea to the continental divide, or to the top of the Apennines in the case of Italy. These air mass circulations create layers over the sea at various altitudes, with accumulated pollutants/precursors in several stages of transformation. These processes can occur during a few consecutive days (e.g. 10 days; Millán et al., 1997). The layers already over the basin descend from 1000–3500 m a.s.l. during the day and can reach the lower levels, providing a high background O_3 to coastal cities when the sea and upslope breezes build up (Millán et al., 2000). Layers, by definition, are stratified and decoupled from each other so they can move in different directions and speeds at their own heights.

Rodriguez et al. (2002) and Cusack et al. (2013) showed that these high background O_3 episodes are characterised also by high particulate matter (PM) concentrations, mostly due to the formation of secondary organic and inorganic aerosols. Such episodes are very common from June to August, and are usually limited by the occurrence of episodic Atlantic or African advective conditions that help (especially the first) to ventilate the western Mediterranean Basin. Minguillón et al. (2015) demonstrated also the occurrence of very intense aerosol nucleation episodes (into the boundary layer) under high-insolation scenarios in the vertical column (from 200 to 1000 m a.s.l.) over the city of Barcelona. As the surface air ascends, aerosols are diluted and levels of O_3 are expected to increase.

The Barcelona metropolitan area (BMA) is a highly industrialised and dense urban agglomeration extending over the Mediterranean side of Northeast Spain. High anthropogenic NO_x and VOC emissions arise both from road (and shipping) traffic and power generation, which, combined with BVOCs emissions, very often cause severe O_3 episodes in the northern plains and valleys (Toll and Baldasano, 2000; Barros et al., 2003; Gonçalves et al., 2009; Seco et al., 2011; Valverde et al., 2016; Querol et al., 2016). The urban plume is transported inland by sea breezes, heading north channelled by N–S valleys that cross the coastal and pre-coastal Catalan ranges to an intra-mountain plain (the Vic Plain) where the cities of Manlleu, Vic and Tona lie, 40–65 km north of Barcelona (Fig. 1). A mean of 15 annual exceedances of the hourly O_3 information threshold/site are recorded at the urban background monitoring sites of these cities (Querol et al., 2016). In 2015, 96 out of the 115 h exceeding the O_3 information threshold in the whole Catalonia air quality monitoring network were recorded in the area within 40–90 km north of Barcelona (towards the Pyrenees), and 82 in the Vic Plain itself (http://www.gencat.cat/mediamb/qaire/ciozo.htm).

This work focuses on an intensive campaign on O_3 and particulate pollutants performed in and around the BMA during July 2015, when high O_3 episodes were recorded, with the aim of investigating the origin of the most intense O_3 events in northeastern Spain. To this end, regional air quality monitoring network data, passive dosimeters at ground level, vertical profile measurements of O_3 and ultrafine particles (UFPs) in the Vic Plain, and modelling tools were employed.

2 Methodology

2.1 Study area

This study is set in central Catalonia (Fig. 1), in northeastern Spain. The mountain ranges surrounding the area (Pyrenees and Catalan coastal ranges) protect the area from the advection of Atlantic and continental air masses but hamper dispersion of pollutants. The typical winds in the region are the tramontana (northern winds), the mistral or cierzo (northwestern winds channelled by the Ebro Valley) and the sea breezes in the coastal region. In summer, daytime upslope winds combined with sea breezes may result in air masses penetrating 120–160 km inland that are injected aloft the top of the mountains, and follow the return night flows towards the sea (Millán, 2014). This scenario of air mass regional recirculation during periods of several days prevails in summer (Millán et al., 1997, 2000). Hence, summer pollution events are characterised by (i) the absence of large-scale forcing and the predominance of mesoscale circulations; (ii) the formation of a thermal low at a peninsular level (forcing the convergence of surface winds from the coastal areas towards the central plateau with strong levels of subsidence over the western Mediterranean Basin); and (iii) combined breeze dynamics, resulting in the recirculation and accumulation of pollutants over the whole western Mediterranean Basin, including the eastern Iberian Peninsula (Millán, 2014; Millán et al., 1997, 2000).

The region is characterised by important atmospheric pollutant emissions from road traffic, industries, biomass burning, livestock, and airport and shipping activities, which coupled with high solar radiation turns into a high rate of secondary PM and O_3 formation (Rodriguez et al., 2002). Industrial activities are mostly concentrated in the Barcelona and Tarragona provinces, and include 19 combustion/energy plants, 84 metallurgy plants and 70 mineral industries. Road traffic, airport and shipping emissions are concentrated in the Barcelona area with $> 3.5 \times 10^6$ vehicles (0.6 per inhabitant, with high diesel and motorbike proportions; DGT, 2014), $> 45 \times 10^6$ tons of shipping transportation, and $> 37 \times 10^6$ aircraft passengers in 2014 (Ajuntament de Barcelona, 2015).

Agriculture, livestock and biomass burning emissions are spread over the rural areas but concentrated in the core study area, the Vic Plain: a 30 km long depression in the north–south direction located 60 km to the north of Barcelona. The area is surrounded by mountains and it is affected by thermal inversions during the night. The summer atmospheric dynamics dominated by sea breezes from the southern sector, channelled through the valleys formed by the coastal ranges, giving rise to the transport of pollutants from the BMA and the numerous surrounding highways.

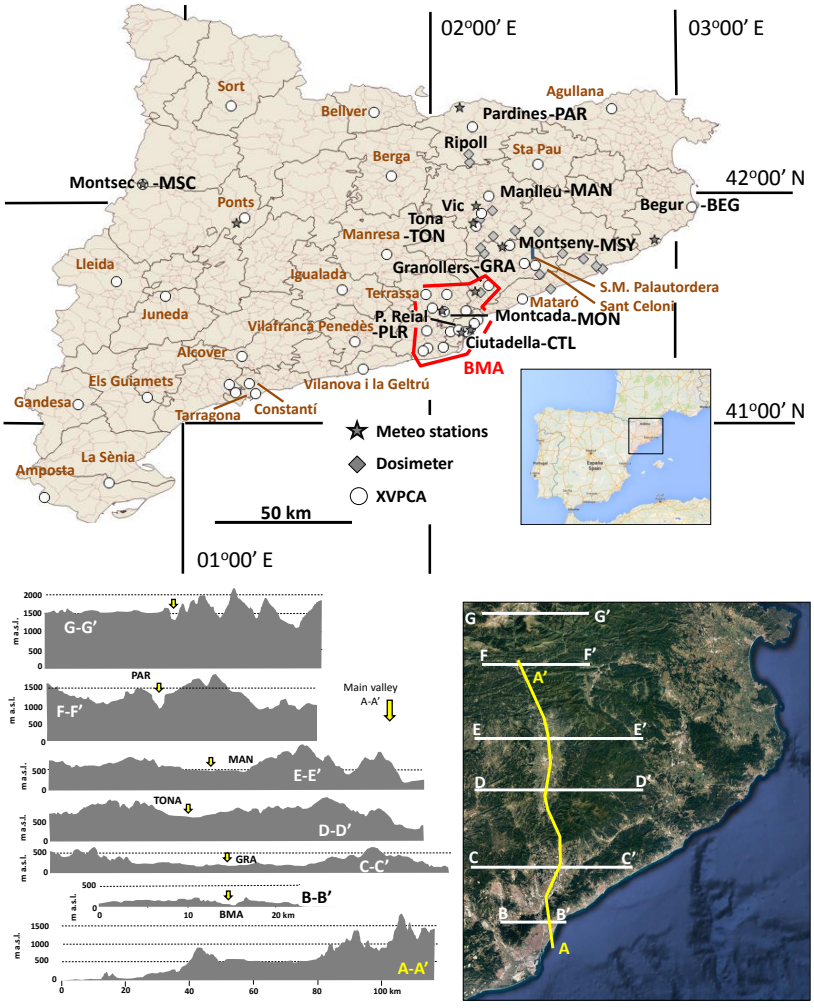

Figure 1. Top: study area and location of monitoring sites (regional air quality monitoring sites XVPCA, dosimeters, meteorological stations and vertical measurements). BMA: Barcelona metropolitan area. Bottom: topographic profiles across the study area, red arrows point to the valleys connecting BMA with the Vic Plain and the pre-Pyrenean regions.

2.2 Ground-level measurements

2.2.1 Online measurements of gaseous pollutants

Measurements of gaseous pollutants were performed at 48 sites belonging to the regional air quality network (Fig. 1, XVPCA; http://dtes.gencat.cat/icqa, Table S1 in the Supplement) from 1 to 31 July 2015. Continuous measurements of O_3, NO, NO_2, CO and SO_2 were carried out using MCV 48AV UV photometry analysers, Thermo Scientific chemiluminescence analysers (42i-TL), Teledyne 300 EU gas filter correlation analysers and Teledyne 100 EU UV fluorescence analysers, respectively.

2.2.2 Measurements of gaseous pollutants with passive dosimeters

Diffusion tubes for NO_2 and O_3 sampling (Gradko Environmental) were deployed at 17 locations between the cities of Barcelona and Ripoll (Fig. 1) covering strategic areas not monitored by the regional air quality network. The dosimeters were positioned along two main river basins in the study area (Besòs/Congost and Tordera), from the BMA to the Vic Plain. Sampling points were selected avoiding the direct influence of vehicular emissions and located at a height of approximately 2.5 m above ground level. One sample per site and sampling period (1–14 and 14–29 July 2015) were collected. After exposure, samples were stored at 4 °C until analysis.

Replicas were placed in nine locations, showing good reproducibility of the results (relative errors of 5 % ± 6 %

for O_3 and $4\,\% \pm 7\,\%$ for NO_2). Dosimeters were collocated also at some XVPCA sites for comparison with reference measurements (6 samples for O_3 at Vic (VIC), Montcada (MON) and Montseny (MSY); and 10 samples for NO_2 at Santa María de Palau Tordera (SMPT), Palau Reial (PLR), Tona (TON), Manlleu (MAN), and Granollers (GRA)). Correction factors were obtained from the comparison between dosimeter and reference data (Dosimeter $O_3 = 1.01 \cdot \text{Reference } O_3 + 17.43$, $R^2 = 0.97$; and Dosimeter $NO_2 = 1.27 \cdot \text{Reference } NO_2 + 1.14$, $R^2 = 0.90$, in all cases in $\mu g\,m^{-3}$) and then applied to the whole dosimeter dataset (Fig. S1 in the Supplement).

NH_3 passive samplers (CEH ALPHA; Tang et al., 2001) were also used in 30 specific points.

2.2.3 O_x concentrations

O_x values ($NO_2 + O_3$) were calculated to complement the interpretation of O_3 concentrations. The concept of O_x was initially proposed by Kley and Geiss (1994) to analyse the O_3 spatial and time variability by diminishing the effect of titration of O_3 by NO ($NO + O_3 \rightarrow NO_2 + O_2$, with the subsequent consumption of O_3) in highly polluted areas with high NO concentrations.

2.2.4 Laboratory van in Vic

A laboratory van was deployed next to the Vic air quality station during the period 10–17 July 2015. Eight-hour $PM_{2.5}$ samples were collected three times per day (00:00–08:00, 08:00–16:00, and 16:00–00:00 UTC) by means of Digitel DH80 high-volume samplers ($30\,m^3\,h^{-1}$) on Pallflex quartz fiber filters (QAT 150 UP). Filters were conditioned at 20–25 °C and 50 % relative humidity over at least 24 h before and after sampling to determine gravimetrically the $PM_{2.5}$ concentration. Subsequently a detailed chemical analysis following the procedure described by Querol et al. (2001) was carried out.

Hourly equivalent black carbon (BC) in $PM_{2.5}$ concentrations were determined by a multi-angle absorption photometer (MAAP, model 5012, Thermo). PM_1, $PM_{2.5}$ and PM_{10} hourly concentrations were determined by an optical particle counter (GRIMM 1107).

2.3 Vertical profiles

During the period 14–17 July 2015 several vertical profiles up to 1550 m a.s.l. (1000 m a.g.l.) were performed by means of a tethered balloon (details can be found in Table S2) in the city of Vic (Fig. 1), at less than 200 m from the laboratory van and the Vic air quality station. The tethered balloon of $27\,m^3$ filled with helium was equipped with an instrumentation pack attached 30 m below the balloon. This setting has been successfully used in previous studies (Minguillón et al., 2015), hence the lack of a fixed support for the instrumentation pack is not expected to hinder the quality of measurements.

The instruments included in the pack were as follows:

- A miniaturised condensation particle counter (Hy-CPC) measuring particle number concentration larger than 3 nm with a time resolution of 1 s and a flow rate of $0.125\,L\,min^{-1}$, using isopropyl alcohol as the working fluid (Lee et al., 2014). The particle number concentration measured by the Hy-CPC will be referred to as N_3. Prior studies have demonstrated the agreement of the Hy-CPC and conventional TSI CPCs (Minguillón et al., 2015).

- A miniaturised nano-particle sizer for the determination of the particle number size distribution (Hy-SMPS, Fig. S2) in the range 8–245 nm with a time resolution of 45 s and a flow rate of $0.125\,L\,min^{-1}$ (Lee et al., 2015). The instrument output agreed well with the results from a scanning mobility particle sizer (SMPS, 10–478 nm), composed of a differential mobility analyser (DMA, TSI 3081) coupled with a CPC (TSI 3772) (Fig. S3, Hy-SMPS $= 0.71 \cdot \text{Reference SMPS} + 999$, $R^2 = 0.88$).

- A miniaturised optical particle counter (Hy-OPC, Fig. S2) measuring particle number concentrations in the ranges 0.3–0.5 µm ($N_{0.3-0.5}$), 0.5–1.0 µm ($N_{0.5-1.0}$), 1.0–2.0 µm ($N_{1.0-2.0}$) and 2.0–5.0 µm ($N_{2.0-5.0}$), with a time resolution of 1 s and a flow rate of $1\,L\,min^{-1}$.

- A microaethalometer (MicroAeth AE51), which provided BC concentrations derived from absorption measurements on a 5 min basis with a flow rate of $0.15\,L\,min^{-1}$.

- A portable O_3 monitor that measures concentrations every 10 s based on UV absorption (POM™ 2B Technologies, Fig. S2). The personal POM O_3 monitor was compared with the O_3 concentrations from the nearby reference station, yielding good results ($n = 34$ min data; POM $O_3 = 0.85 \cdot \text{Reference } O_3 + 0.56$, $R^2 = 0.93$) (Fig. S1). The measured vertical O_3 concentrations reported in this study were normalised to standard temperature and pressure conditions (25 °C, 1013.2 hPa).

- A global positioning system (GPS).

- Temperature, relative humidity, pressure, wind direction and wind speed sensors.

A further sounding was carried out on the 16 July 2015 at 11:00 UTC. A free balloon was used with an instrumentation pack equipped with a Hy-CPC, a GPS, a temperature sensor and a relative humidity sensor. The pack was placed in an insulated box (Fig. S4).

2.4 Meteorological parameters

The 30 min meteorological data from 11 sites located throughout the study area in the proximity of air quality monitoring sites were provided by Meteocat (Meteorological Office of Catalonia) (Fig. 1 and Table S3). Hourly average wind components were calculated and used in polar plots with hourly O_3 and O_x concentrations, by means of the OpenAir software (Carslaw, 2012). These are bivariate polar plots where concentrations are shown to vary by wind speed and wind direction as a continuous surface.

2.5 Modelling system for O_3

The ambient O_3 concentrations were modelled using the ARAMIS (A Regional Air Quality Modelling Integrated System) high-resolution modelling system that integrates the Weather Research and Forecasting model (WRF-ARW) version 3.1.1 (Skamarock et al., 2008) as a meteorological model, the High Resolution Emission Model (HIREM) (Soler et al., 2004, 2011, 2015) and the Models-3 Community Multiscale Air Quality Modelling System (Models-3/CMAQ) (Byun and Ching, 1999) as a photochemical model. The modelling system was configured using four nested domains: D1, D2, D3 and D4 with horizontal grids of 27, 9, 3 and 1 km, respectively. For the coarser domain, initial and boundary conditions for the meteorological model were taken for the European Centre for Medium-Range Weather Forecast (ECMWF) global model with a $0.5° \times 0.5°$ resolution using nudging and the boundary conditions are forced every 6 h, whilst for the photochemical model initial and boundary conditions model came from a vertical profile supplied by CMAQ itself. Domains are run in one-way nesting and 24 h spin-up was performed to minimise the effects of initial conditions for the inner domains. The output data are saved every hour. ARAMIS is continuously updated, and has been extensively evaluated (Soler et al., 2015) to simulate air quality over regional and local scales. In the present study the domain D3 was used, which covers the area of interest.

3 Results and discussion

3.1 Meteorological background and diurnal cycles of pollutants

Two types of episodes that will be discussed in the following sections were identified concerning the meteorological patterns and the O_3 concentrations recorded.

Type A episode. Under "usual summer conditions", with the Azores High located west of Iberia, and a ridge of high pressures extending into southern France, air masses in the western Mediterranean Basin rotate clockwise (anticyclonic) during the day, following the combined sea breezes and upslope flows at eastern Iberia and a simultaneous generalised compensatory sinking is observed in the basin. During nighttime, drainage flows into the sea develop at the coastal strip, subsidence over the basin weakens and the wind over the sea is observed moving southward, transporting the coastal emissions almost parallel to the shoreline (Gangoiti et al., 2001). At the same time, Atlantic gap winds (through the Ebro and Carcassonne valleys), weaken during daytime due to inland sea breezes and become strengthened during nighttime (Millán et al., 1997; Gangoiti et al., 2001, 2006; Millán, 2014). In such conditions, the air layers over the sea in front of Barcelona tend to move within the southwesterlies during the day, following the clockwise rotation, i.e. towards southern France and the Gulf of Genoa, and within the northerlies (towards Valencia) during the night. Thus, direct transport of O_3 and precursors from the Fos–Berre–Marseille–Piombino (Livorno) area towards the BMA is weak or null. However, indirect transport is more likely, first into the sea during nighttime conditions, and then following the daytime southwesterlies for the combined coastal sea-breeze and anticyclonic gyre at the coastal strip of Catalonia, which could bring a fraction of the referred O_3 and precursors originated in southern France, together with those emitted at the eastern coast of Iberia.

Type B episode. When the anticyclone establishes over central Europe with relative low pressure to the west over the Atlantic, the flow pattern over the western Mediterranean changes: southerly winds blow at height over eastern Iberia, while at ground level, gap winds may weaken or stop the Mistral and the tramontana winds in the Gulf of Lion, and Barcelona could then be directly affected by O_3 and precursors, coming with the easterlies blowing at the marine boundary layer (emissions from Corsica, Sardinia and Italy). However, under these atmospheric conditions O_3 levels did not reach the observed values found during type A episodes, and the O_3 daily records did not show the classical pattern of accumulation from one day to the next, characteristic of the highest O_3 episodes in the western Mediterranean (Millán et al., 1997, 2000; Castell et al., 2008a).

Under the above "usual summer conditions", Millán et al. (1991, 1996a, b, c, 1997, 2000, 2002), Gangoiti et al. (2001) and Castell et al. (2008a) demonstrated the vertical recirculation of O_3-rich masses in the western Mediterranean, with O_3 being formed from precursors transported inland by the combined upslope and sea-breeze winds. O_3 loaded air masses, elevated by topography and sea-mountain breezes will be transported back to the coastal area at a certain altitude during the day and accumulates in elevated stably stratified layers at the coastal areas during the late evening and night. During nighttime and at ground level O_3 depletion dominates mainly in urban and industrial centres, driven by reaction with new emissions, which at the coastal area are transported offshore within the stable surface drainage flows.

The synoptic atmospheric situation in July 2015 was characterised by an intense high-pressure system over central and southern Europe during almost the whole month (Fig. 2).

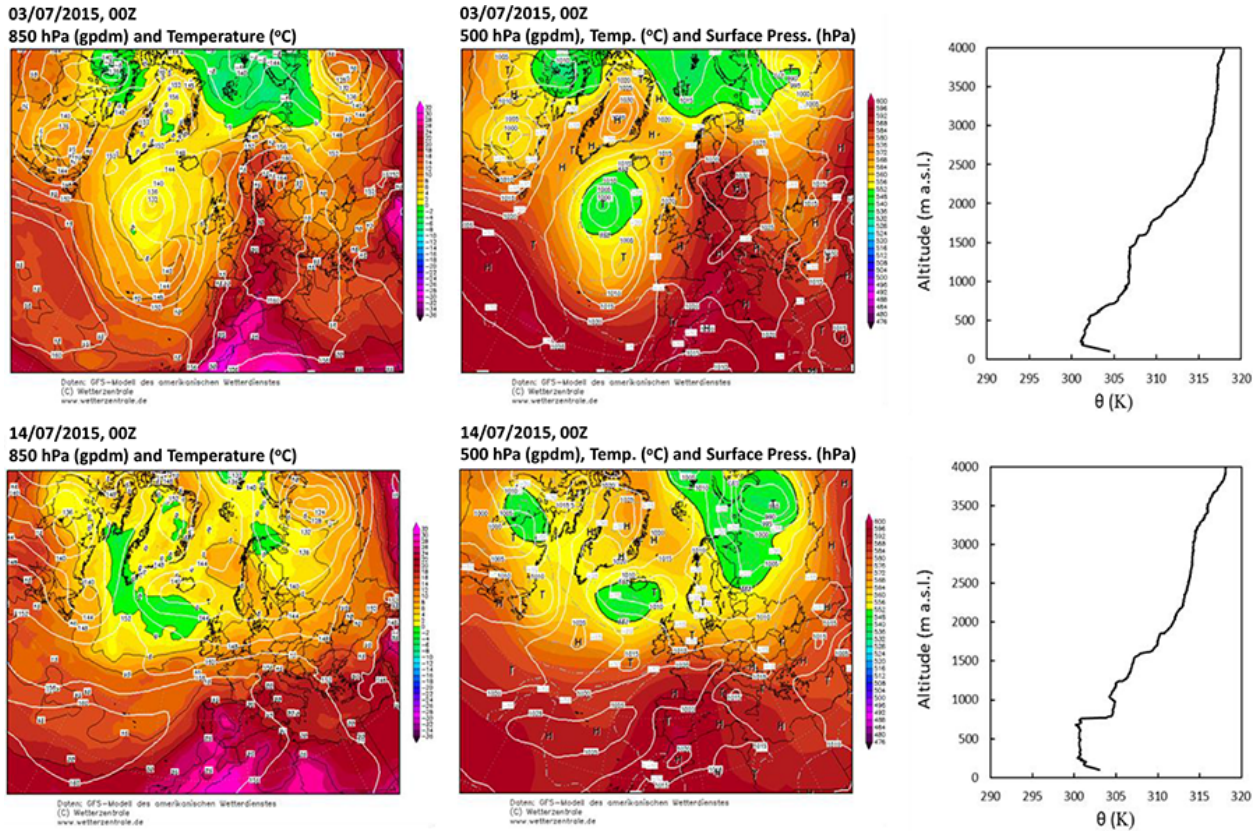

Figure 2. Geopotential and temperature at 850 hPa (left) and 500 hPa (centre). Potential temperature (K) of the atmospheric sounding in Barcelona (WMO 08190) at 12:00 UTC (right). Meteorological figures are reported for 3 July 2015 (top) and 14 July 2015 (bottom).

Type A and B scenarios alternated, transporting warm air masses from North Africa towards higher latitudes by the anticyclonic dynamic and reaching extremely high temperatures in Europe. The stagnation of air masses induced a regional meteorological scenario in the area under study, characterised by local/regional recirculations and sea–land breezes, both channelled by the complex topography. The flow pattern, together with the observed stably stratified layers developed up to a height of 2000–2500 m a.s.l. (Fig. 3) associated with subsidence, enhanced the accumulation of pollutants and caused several pollution episodes in the north-eastern Iberian Peninsula. Coastal and pre-coastal locations (Barcelona) were mainly affected by daily sea breezes, starting blowing from the east (around 08:00 UTC) and turning progressively to the south and southwest. The sea breezes were channelled through the valleys, which are mainly located following a north-to-south axis, and arrived at the monitoring stations predominantly from a southerly direction. However, during the night atmospheric conditions were much more stable with flow patterns dominated by land breezes from NNW.

The VIC site was characterised by stagnant conditions during the day, reaching the maximum wind speed (4 m s^{-1} on average) at around 15:00 UTC, when sea-breeze intensity was at the highest (Fig. 4). During the night very light winds blew from the north (Fig. 4). During the periods 14–20 July 2015 (episode type A) and 3–6 July 2016 (episode type B) the sea breeze blew from 10:00 to 18:00 and 10:00 to 21:00 UTC, respectively, but in the first episode the wind speed was higher (maximum of 2.7 m s^{-1} as an average for the period) and maximal at 14:00 UTC, whereas in the second wind speed was lower, with a maximum mean value for the period of 2.4 m s^{-1} at 17:00 UTC, but only 1.5 m s^{-1} at midday.

Averaged ground O_3 concentrations during the type A episode recorded at VIC were clearly influenced by these wind patterns, showing a typical midday peak, followed by a higher peak at 13:00–14:00 UTC probably caused by the transport of BMA air masses by the breeze (Fig. 4). Mean O_3 levels during this A episode reached 195 µg m^{-3} at 13:00 UTC. During the type B episode average O_3 levels were also very high (142 µg m^{-3} at 14:00 UTC) but clearly lower than during the A episode (Fig. 4).

Intensive surface measurements were only available for 10–17 July 2015 (when the mobile laboratory was working at VIC). Average SO_2 levels for this period (included in the type A episode) showed a similar daily pattern to that of O_3 (Fig. 4) pointing to a probable Hewson type I fumigation

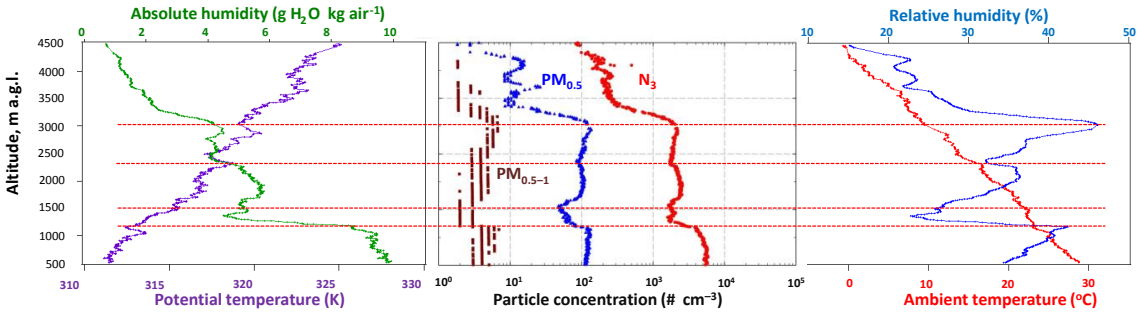

Figure 3. Data from the non-tethered balloon measurements (at VIC) of temperature, relative humidity and particle number concentrations performed from 10:00 to 11:30 UTC on 16 July 2015. Red lines identify the limit between different atmospheric layers.

process (Hewson, 1964; Geiger et al., 1992); when midday convective flows that abate the surface a SO_2-rich layer accumulated in the limit of the boundary layer. Ground-level concentrations of BC, NO_2 and PM_x showed a similar daily pattern driven by stagnation and traffic rush hour, with maximum concentrations around 06:00 UTC (08:00 local time, Fig. 4). Finally, extremely high concentrations of NH_3 (this is one of the most intensive farming regions of Spain and mean values of the Vic Plain dosimeters reached 30 µg m^{-3} NH_3 for 1–31 July 2015) followed the typical midday maximum due to evaporative emissions from fertilisers, but the rapid increase of the wind speed and dilution by the growth of the planetary boundary layer (PBL) thickness (see vertical profiles of temperature, aerosols and O_3 at VIC in following sections) probably account for a relative reduction of ground-level NH_3 concentrations during the central hours of the day (Fig. 4).

The varying diurnal and nocturnal air mass patterns in the Vic Plain are also shown by the $PM_{2.5}$ chemical composition. Figure S5 shows the 8 h concentration patterns of selected components during the week period of 10–17 July 2015, including several days (14 to 17 July 2016) of the type A episode defined above, affected by polluted air masses from the BMA.

In addition to the regionally transported O_3, concentrations of elemental carbon (EC) and traffic and industry-related metals (including Zn, Cu, Pb, Sn and Sb) were notably enhanced at the end of the week, and were attributed to local sources. This enhancement was most obvious during the 00:00–08:00 UTC period (Fig. S5), under calm or northerly low wind (drainage slope winds) carrying metallic pollutants from the Cu smelter located 13 km to the north of Vic, and leading to high Cu, Zn, Sn, W, Pb and Sb concentrations on the nights of 15 and 16 July 2015 (Fig. S5). The increase in EC was related to local traffic emissions during the morning rush hour as deduced from the peaking MAAP BC concentrations during 05:00–08:00 UTC (07:00–10:00 local time), up to 5 µg m^{-3} hourly BC, when compared to 3 µg m^{-3} recorded as maximum traffic rush hour concentrations in the preceding days (data not shown). In contrast, the rise of organic carbon (OC) concentrations observed during 08:00–16:00 UTC is attributed to the formation of secondary organic aerosols.

Sulfate concentrations did not show any trend, as expected from secondary inorganic components present in relatively homogeneous concentrations on a regional scale, whereas nitrate (and partially of ammonium) concentrations increased during the 00:00–08:00 UTC periods as a result of gas to particle partitioning (Fig. S5) due to the thermal instability of ammonium nitrate (Hertel et al., 2012), under typical high daytime temperatures reached in July 2015. Interestingly, the stronger southerly winds during the daytime in the second part of the week (see below) appear to have brought polluted air from the BMA as signalled by slightly higher V concentrations (tracer of fuel oil combustion), but the fumigation from high strata (polluted air masses that were injected the previous day or days) might also account for these SO_2 and V increases.

The concentrations of mineral matter and all its components (Al, Fe, Mg, Li, Ti, Rb, Sr, Ti) were constant during the week, with relatively higher concentrations in the 08:00–16:00 UTC samples (Fig. S5), indicating a higher resuspension caused by stronger afternoon winds. The increment on the 15 July 2015 (08:00–16:00 UTC) was attributed to resuspension of local dust, given that the occurrence of African dust outbreaks was not observed during this period.

The free sounding measurements carried out at 11:00 UTC on 16 July 2015 revealed stratified air masses up to 3000 m a.g.l. (Fig. 3). The vertical profiles of potential temperature, water vapour and aerosol concentration distributions can be used for the identification of atmospheric layers presenting different properties: a lower layer up to about 1100 m a.g.l. characterised by a relatively high aerosol concentration, well mixed and with a relatively high and uniform water vapour content. A clear discontinuity between 1100 and 1500 m a.g.l. limits the mentioned lower layer and a series of stably stratified layers up to a height of 3000 m a.g.l. This layering of pollutants is probably related to the development of regional and mesoscale convective cells driven by the

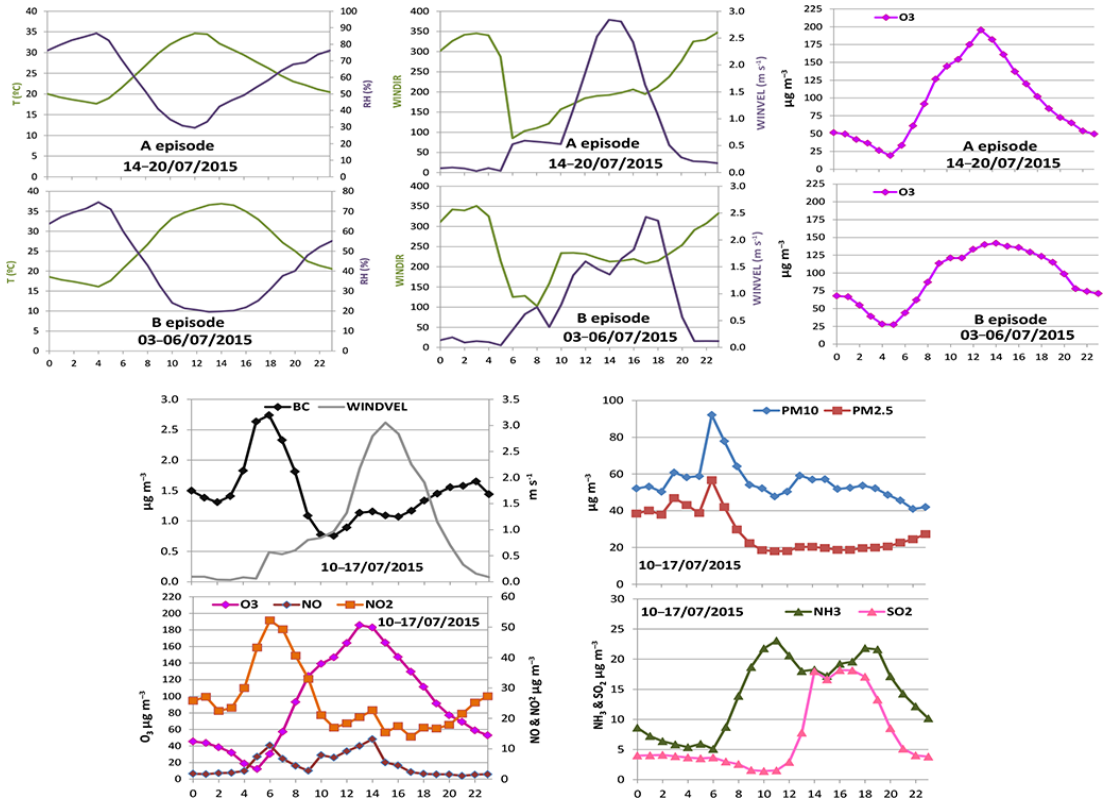

Figure 4. Top: mean hourly (UTC) values for meteorological parameters and O_3 ambient air concentrations measured during the periods 3–6, 14–20 and 10–17 July 2015 recorded at the permanent VIC XVPCA station (O_3) and at the Gurb meteorological station (temperature, humidity and wind patterns, Meteocat) located 1 km to the north of VIC. Bottom: mean hourly concentrations of other gaseous and particulate pollutants measured at VIC with the laboratory van (only during the period 10–17 July 2015) co-located with the XVPCA station.

combined upslope and sea-breeze flows developed the day before (Millán et al., 1997).

3.2 O_3 and O_x episodes

Figure S6 shows the average O_3 and O_x ground-level concentrations recorded in July 2015 in the study area at the XVPCA air quality monitoring network and with the passive dosimeters. O_x maximum concentrations were recorded at the Vic Plain area and in the coastal sites northeast of Barcelona. This may be due to the high O_3 concentrations in Vic and to a higher proportion of primary NO_2 (emitted mainly from diesel engines, and not formed in the atmosphere from NO titration by O_3) in the coastal cities, respectively.

In July 2015, the O_3 hourly information threshold was exceeded a total of 74 times at the XVPCA stations of Catalonia, 57 taking place in the Vic Plain stations (TON, VIC and MAN), and 69 in the surrounding areas (pre-Pyrenees, High Llobregat River and Montseny).

Figure 5 shows hourly O_3 concentrations for the study period from selected monitoring sites. O_3 concentrations recorded at a coastal (Begur, BEG; blue, 200 m a.s.l.) and a remote inland western pre-Pyrenean site (MSC, light green, 1570 m a.s.l.) (Fig. 5a) show relatively narrow diurnal variations and multiday episodes, with low or enhanced concentrations, according to meteorological fluctuations (accumulation and air mass renovation cycles of 3 to 12 days cause a wider O_3 and O_x concentrations range than the typical daily cycles evidenced in most of the other sites). O_3 variations at the coastal BEG are opposed, in periods such as 1–3, 10–12 and 26 July 2015 and several periods from 14–20 July 2015, to those at the inland MSC. As shown by the polar plots from Fig. 6, relatively low O_3 concentrations (but still high in absolute terms) were recorded at the BEG coastal site (easternmost site in this figure) when the wind blows from the sea, whereas polluted air masses are transported towards the inland remote MSC (westernmost location in the figure) site under the same meteorological conditions. Conversely, when westerly winds blow, the inland remote MSC site received relatively clean air masses with low O_3 (Fig. 6), which are progressively loaded with regional pollution as these are transported towards the coastal BEG site.

Data from two urban background sites of Barcelona (PLR and CTL, 81 and 5 m a.s.l., grey and black in Fig. 5b) show evidence of a high nocturnal O_3 consumption, with differences due to local NO_x traffic emissions. Following the trans-

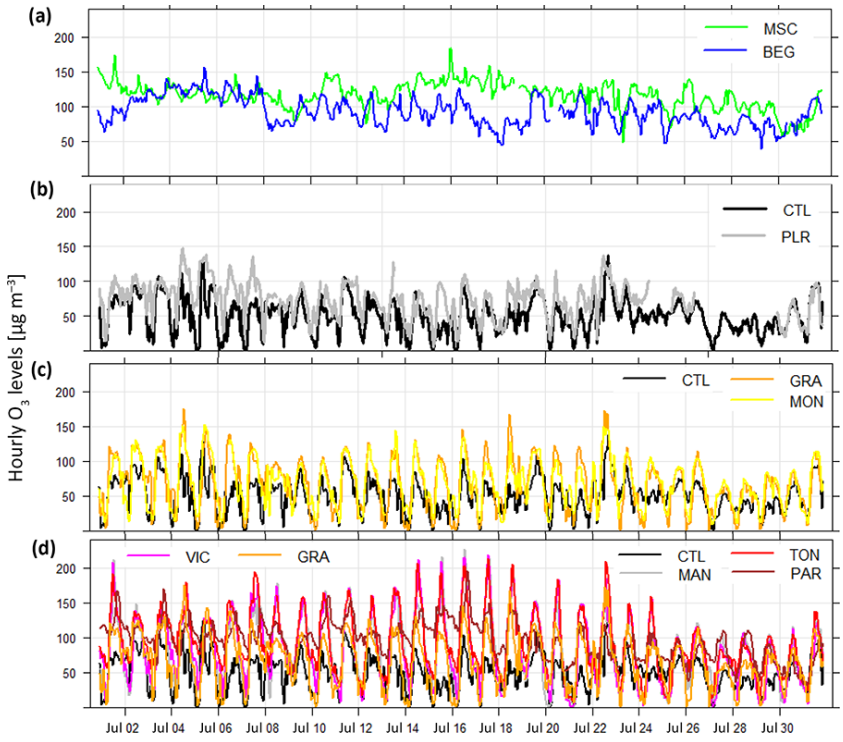

Figure 5. O_3 hourly concentrations recorded at the coastal (BEG, blue) and remote inland western pre-Pyrenean (MSC, clear green, 1570 m a.s.l.) sites, two urban background sites of Barcelona (PLR, CTL, grey and black), two urban sites in the northern periphery of Barcelona metropolitan area (GRA, MON, orange and yellow), the inner Vic Plain sites (TON, VIC and MAN, red, pink and violet) and the remote eastern pre-Pyrenean site of PAR (brown), during July 2015.

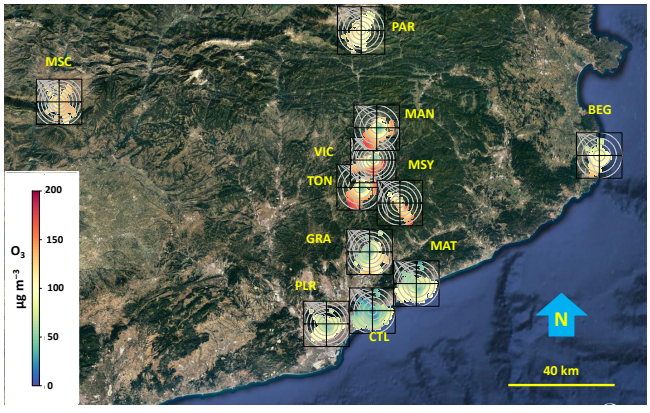

Figure 6. Polar plots of hourly O_3 concentrations at the real-time measurement sites.

port of air masses by combined breezes, the two sites located in the northern periphery of the BMA, along the Besòs River valley (GRA and MON, 140 and 33 m a.s.l., orange and yellow in Fig. 5c; 20 and 6 km from BMA in NE an NNE directions, respectively) show local O_3 production, with higher midday concentrations, while very low nocturnal levels reflect again the intensive O_3 consumption (in a densely populated basin). O_3 concentrations were closer between GRA and MON than between the two Barcelona urban sites (PLR and CTL).

Relevant O_3 net production and fumigation can be readily seen in the inner Vic Plain (TON, VIC and MAN; 620, 498, 460 m a.s.l.; red, pink and violet in Fig. 5d; 45, 55 and 62 km from BMA in a NNE direction, respectively) as well as at the remote eastern pre-Pyrenean site of Pardines (PAR, brown, 1226 m a.s.l., 102 km from BMA in a NNE direction), where O_3 formation and fumigation seems to have already reached its maximum, and similar O_3 concentrations were recorded at all sites during the midday increase. This suggests that the intensity of O_3 formation and fumigation was clearly reduced in the Vic Plain–Pyrenees transect with respect to the Barcelona–Vic Plain (an intermediate production place would be MSY (720 m a.s.l.; green in Fig. 7, 39 km from BMA in a NE direction). Polar plots of GRA, TON, MSY, VIC, MAN show clearly that the highest O_3 levels were recorded with wind blowing from the direction where BMA is located (Fig. 6).

As can be observed in Figs. 5 and 7, during two periods (1–2 and 7–20 July 2015) O_3 concentrations increased progressively from Barcelona city towards the northern BMA (GRA and MON), the intermediate MSY regional background area and towards the northern Vic Plain sites; and from there it slightly decreased towards the eastern pre-Pyrenees (PAR)

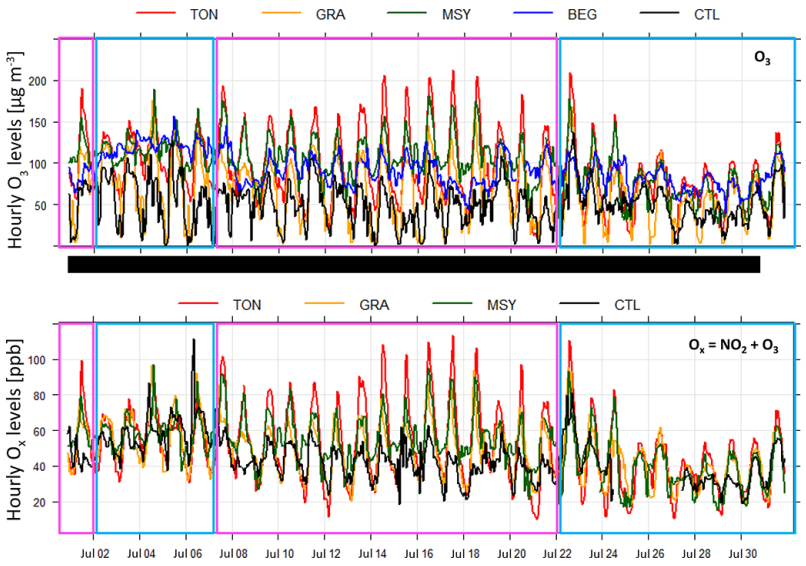

Figure 7. O_3 and O_x ($O_3 + NO_2$) hourly concentrations recorded at the coastal (BEG, blue, at this site only O_3 is available due to the lack of NO_2 measurements), an urban background site of Barcelona (CTL, black), an urban site in the northern periphery of Barcelona metropolitan area (GRA, orange), the intermediate inland rural site of MSY (720 m a.s.l., green), and the inner Vic Plain site (TON, red) during July 2015. The pink and blue squares mark the A and B O_3 and O_x episodes distinguished in this study, respectively.

following the midday–afternoon combined breeze transport (Figs. 5 and 7). During these days, no exceedance of the information threshold was produced in the urban environment; only sporadic peak concentrations above the human protection target value were recorded in the close surroundings of Barcelona. However, frequent exceedances of both thresholds were recorded in a regional transport context towards the north of the BMA.

While differences in O_3 concentrations between TON, GRA, MSY, BEG and CTL were observed during the period 3–6 July 2015 (type B episode), O_x concentrations show a very similar behaviour along the Vic Plain, both qualitatively and quantitatively (Fig. 7, O_x is not reported at BEG due to the lack of NO_2 measurements). Conversely, in the period 7–20 July 2015 (which includes the type A episode), characterised by a change in the synoptic conditions, differences in daily maximum O_x values resemble the same behaviour of O_3 alone, with a positive and marked inland gradient. O_3 concentrations at BEG, a coastal site far in the northeast, were higher during the former period and showed low intra-day variation, indicating probable long-range transport of polluted air masses (Fig. 7).

O_3 and O_x concentrations at the regional background site (MSY, 720 m a.s.l., green in Fig. 7) depict also the meteorologically influenced patterns (in the sense previously described for BEG and MSC), but with a clear overlapped and pronounced daily fluctuation, with marked higher concentrations indicating O_3 generation from a regional origin and fumigation from upper layers,, especially on 1–2 and 7–20 July 2015 (Fig. 7).

Diurnal O_3 concentrations in the Vic Plain (around 460–620 m a.s.l.) were markedly higher than at the coastal (CTL, PLR) sites, and slightly higher than at mountain sites (MSY, PAR and MSC, from 720, 1226 and 1570 m a.s.l.) during the 1–2 and 7–20 July 2015 periods. The O_3 hourly information threshold of 180 µg m^{-3} was exceeded 55 times in the Vic Plain (three sites), with 50 of these exceedances taking place during 1 July 2015 and 14–20 July 2015. For these exceedances, an hourly contribution of up to 150 µg m^{-3} of O_x (mostly O_3) both from fumigation of recirculated return layers (injected at an altitude of 1500–3000 m a.g.l. in the prior day(s)), and from transport and photochemical generation of O_3 of the BMA plume, might be estimated based on the differences of the O_x early afternoon maxima recorded at the coastal BMA sites (CTL, PLR) and the ones in the Vic Plain (TON, MON, VIC). Thus, as shown in Fig. 7, the 14–18 July 2016 midday maxima recorded at CTL (into BMA) range between 38 and 62 ppb O_x, on an hourly basis, whereas at TON (in the Vic Plain) they reach 102–115 ppb. Accordingly, differences of 50–73 ppb O_x (close to 100–150 µg m^{-3} O_x) between CTL and TON can be estimated for these days. Furthermore, different intensity and duration of fumigation from upper high O_3 layers might also contribute to the higher inland O_3 surface concentrations since the PBL depth is much higher at the inland Vic Plain than at the coastal site, where sea breeze flows favour a lower growth of the PBL.

3.2.1 Type A episode (14–20 July 2015)

During this episode, a progressive time shift of the daily hourly O_3 and O_x maxima was observed from the Barcelona

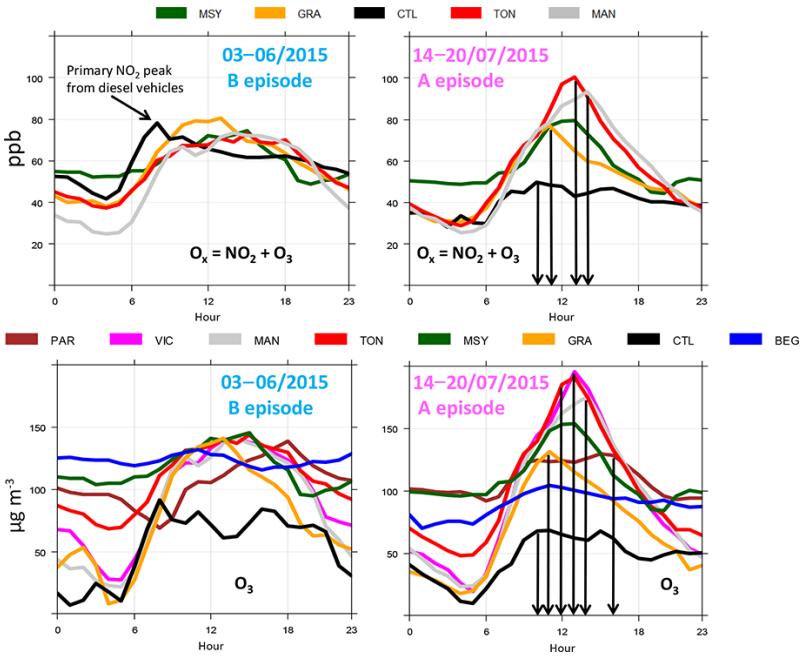

Figure 8. Mean hourly levels of O_3 and O_x ($O_3 + NO_2$) for sites in a south (coast) to north (inland) transect (CTL, GRA and BEG, and MSY, TON, VOIC, MAN and PAR, respectively) following the inland transport of pollutants from the coast, and maxima time shift according to the sea-breeze transport (right) for the periods 3–6 July 2015 (B type episode, left) and 14–20 July 2015 (type A episode, right). Time is UTC.

area (10:00 UTC, at CTL into the BMA) towards the metropolitan periphery (11:00, at GRA), the intermediate mountain sites (13:00, MSY, 39 km from BMA), the Vic Plain (12:00, 13:00 and 14:00, TON, VIC and MAN, 45, 55 and 62 km from the BMA, respectively) and the northern pre-Pyrenean site (16:00, PAR, 102 km from BMA) (Fig. 8). As described above, this variation points to the process of O_3 and O_x formation with a mean O_x difference between the urban-coastal sites and the Vic Plain hourly maxima of up to 73 ppb O_x (around 150 $\mu g\,m^{-3}$) for the TON site when O_x hourly maxima from CTL are subtracted (Fig. 7), with maximum average O_3 hourly levels of around 200 $\mu g\,m^{-3}$. These O_x differences are mostly due to O_3 differences (Fig. 8). Accordingly, during these intense O_3 pollution episodes, more than 50 % of the O_x and O_3 hourly maxima concentrations are attributable to (i) O_3 contributions from the previously mentioned surface fumigation of recirculated strata (over the VIC–MAN–TON area) containing the polluted air masses injected the day before by complex topographically induced circulations, and to (ii) the local O_3 generation and surface transport of the BMA plume into inland valleys. Attributing these O_3 exceedances to local/regional causes is also supported by the spatial distribution of the hourly O_3 maxima, the number of hourly exceedances of the information threshold, the time shift of the exceedances at the different sites (as moving towards the north) (Fig. 9), and the polar plots of hourly O_3 concentrations pointing towards BMA as the main source region (Fig. 6). It is important to note that, as previously stated, in the coastal sites the PBL height is markedly reduced when compared with the inland regions and then the capture of these high-altitude O_3-rich layers by the PBL growth and the consequent fumigation on the surface is less probable in the coastal areas than in the inland ones.

Thus, during the A episode, O_3 has mostly a major local/regional origin (with O_x maximum hourly levels progressively increasing from 166 to 246 $\mu g\,m^{-3}$ from the BMA to the Vic Plain). The concatenation of daily cycles of regional/long-range recirculation of air masses and regional/local O_3 production in the A episode accounted for the accumulation of O_x and the consequent exceedance of the hourly information threshold. Castell et al. (2008a) have already reported a correlation between their "recirculation factor" (a meteorological parameter devised to increase with the concatenation of days with regional vertical recirculation of air masses) with the occurrence of O_3 episodes in 2003. The relevance of these recirculations in originating these high O_3 episodes in southern Europe has been highlighted already, not only by scientific papers by the CEAM team but also assumed by the European Commission (EC, 2004).

Figures 10 and 11 show results for the vertical profiles (0–1100 m a.g.l.) of O_3 concentrations, particle number concentrations for particles > 3 nm (red), 0.3–0.5 μm (blue), 0.5–1.0 μm (brown), ambient temperature, relative humidity and wind direction, obtained at the beginning of the type A episode (from 14 to 17 July 2015).

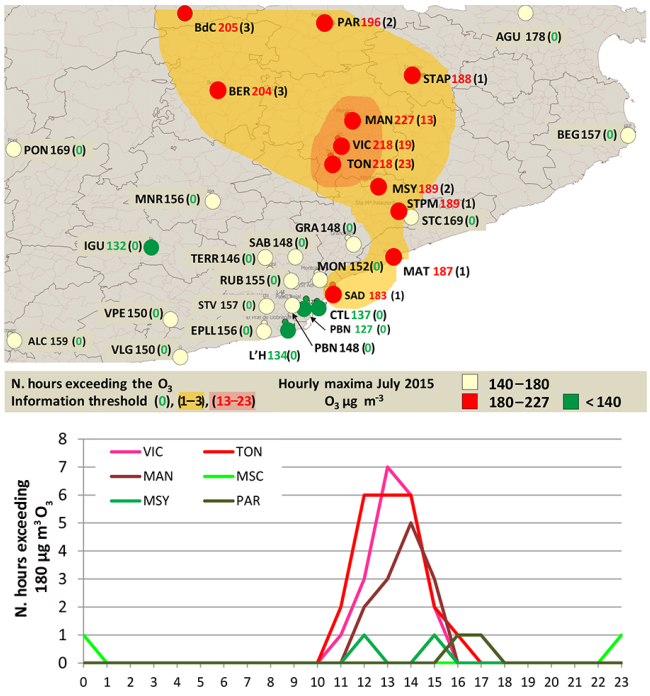

Figure 9. Top: hourly O_3 maxima (and number of hours exceeding 180 µg m^{-3}) in the study sites with real-time O_3 measurements (shadowed areas indicate two different degrees of exceedances, 1–3 and 13–23 h). Bottom: frequency of occurrence of hourly (UTC) O_3 exceedances of 180 µg m^{-3} along the day; both for July 2015.

In the profiles from 07:06 to 08:21 UTC on 14 July 2015, a boundary layer (150 to 250 m thick) with relatively high levels of N_3 (0.8 to 2.0 × 10^4 cm^{-3}) was differentiated from the free troposphere (0.2 to 0.8 × 10^4 cm^{-3}) (Fig. 10). However, in the profile obtained from 09:42 to 10:52 UTC on 17 July 2015, the growth by convective turbulence accounts for a homogeneous boundary layer and profile of $N_{0.3-0.5}$ below 1000 m a.g.l. (Fig. 10). Inside the PBL nucleation occurred (yellow to red areas in Fig. 12 for 16 July 2015) regionally driven by photochemical processes. Minguillón et al. (2015) showed the occurrence of these nucleation events into the PBL as convective transport elevates and dilutes air masses from polluted areas under high insolation in Barcelona. During the period 14–16 July 2015 nucleation episodes occurred occasionally, but only inside the PBL. On 17 July 2015 at 09:42–10:52 UTC new particle formation occurred probably at relatively high altitudes, also inside the PBL, as deduced from the high N_3 levels measured from 400 to 1000 m a.g.l., with concentrations reaching 1 × 10^4 cm^{-3}, while simultaneously low concentrations (< 0.3 × 10^4 cm^{-3}) were measured at ground level (Fig. 10). This vertical gradient is not observed for the coarser particles ($N_{0.3-0.5}$ and $N_{0.5-1}$) and O_3 (Figs. 10 and 11, for which relatively constant levels were measured inside the PBL), suggesting new particle formation.

On 14 July 2015 at 07:06–08:21 UTC a well-stratified atmosphere (Fig. 11) with both thermal and O_3 layers is observed, with a general upward increasing trend for O_3 from 40 µg m^{-3} at ground level to much higher levels in different strata, one reaching 150 µg m^{-3} in strata at 500 m a.g.l. and others of 140, 100 and 40 µg m^{-3}, at 300, 800–1000 or 400 m a.g.l. respectively, reflecting, in addition to stratification of O_3 concentrations in altitude, the effect of surface depletion by NO titration and by deposition during the night (see in Fig. 11 the progressive O_3 depletion from 150 µg m^{-3} at 500 m a.g.l. to 40 µg m^{-3} at surface levels). From 13:49 to 15:03 UTC on 14 July 2015 (Fig. 11) the vertical profile changed substantially, with an already unstable atmosphere near the ground, showing very high surface O_3 concentrations of 217 µg m^{-3} that increase up to 330 µg m^{-3} in a layer around 100 m a.g.l., decreasing again through an upper layer with values of 240 µg m^{-3} until 300 m a.g.l. (where measurements were not available due to instrumental problems). This 100–200 m a.g.l. high O_3 layer agrees with the modelled O_3 concentrations for the study area (Toll and Baldasano, 2000; Barros et al., 2003; Gonçalves et al., 2009) and reflects elevated O_3 concentrations due to local production and transport of O_3, that decrease from 100 m a.g.l. to the surface due to its titration, consumption and deposition. On 15 and 16 July 2015, a similar upward increasing O_3 gradient was observed in the early morning (Fig. 12). On 17 July 2015 at 07:39–08:40 UTC O_3 concentrations were relatively constant, but also showed a strongly stratified profile, in the range of 100–165 µg m^{-3} in the lower 500 m. In the last profile, from 09:42 to 10:52 UTC, O_3 concentrations increased from 140 to 200 µg m^{-3} for 200 to 1000 m a.g.l., but again a maximum close to 200 µg m^{-3} was observed at the same height around 100 m a.g.l. (Fig. 11).

Thus, vertical profiles of the type A episode are characterised in the early morning by a strong stratification, showing low ground-level O_3 concentrations, due to low production (low insolation) and/or consumption (titration and deposition), and increasing concentrations with altitude. This variation is related to prevailing meteorological conditions enhancing local recirculation or larger-scale transport with high O_3 masses injected (the day before) at certain altitudes by vertical recirculations into the residual layer, above the nocturnal surface stably stratified boundary layer. Nevertheless, during specific days, homogeneous O_3 vertical profiles up to 1000 m a.g.l. (the maximum height reached with captive sounding) were also evidenced, but probably not maintained at higher levels (where we were not able to measure with our system). Thus, as shown by the 4500 m profile measured with the free sounding on 16 July 2016 (Fig. 3), high PM (and probably O_3) strata are present between 1500 and 3000 m a.g.l., these being probably the polluted air masses injected the day before in the northern mountain ranges and recirculated to the coast at certain altitudes (see modelling outputs below). On the other hand, with constant southerly winds (from the coastal area to the Vic Plain)

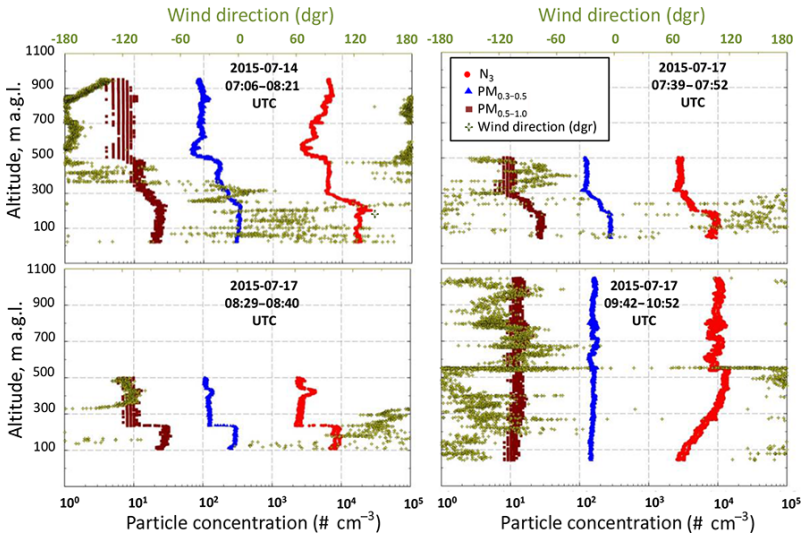

Figure 10. Vertical profiles of particle number concentrations for particles > 3 nm (red, N_3), 0.3–0.5 µm (blue, $PM_{0.3-0.5}$), 0.5–1.0 µm (maroon, $PM_{0.5-1}$) and wind direction obtained with the tethered balloon measurements on 14 and 17 July 2015.

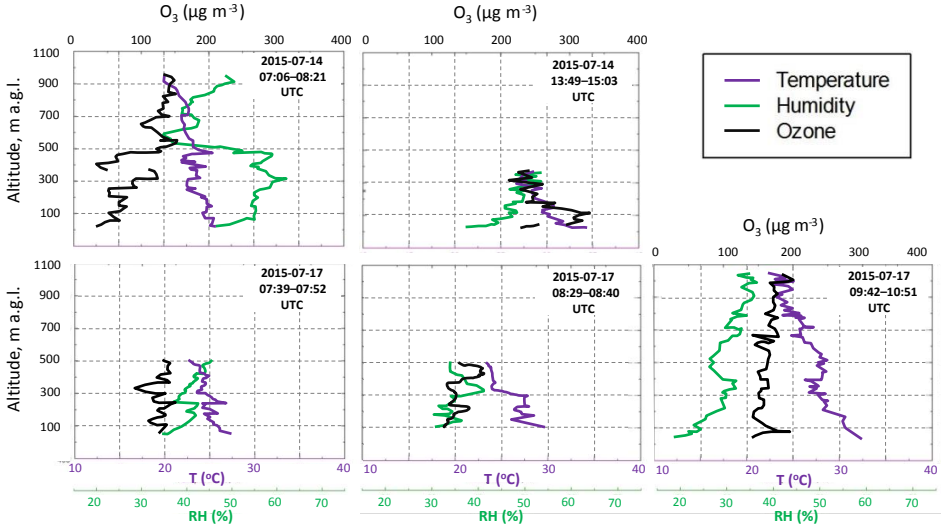

Figure 11. Vertical profiles of O_3, temperature and relative humidity obtained with the tethered balloon measurements on 14 and 17 July 2015.

usually associated with the combined sea-breeze and upslope flows, O_3 was enriched in the lower 100–200 m atmospheric layer, generated by the intensive local photochemical production. O_3 concentrations reached maximal values (up to 330 µg m^{-3}) on the top of this layer, while they decreased at lower heights by titration and deposition, although hourly levels of 225 µg m^{-3} were still recorded. These results are consistent with the gradient of O_3 concentrations between the Vic Plain (around 500 m a.s.l.) and the MSY mountain site (720 m a.s.l., and closer to the sea) during the episodes (Figs. 7 to 9). At higher altitude, O_3 concentrations slightly decreased but were still high (150–240 µg m^{-3}) due to the O_3 formation in air masses constantly transported from the coastal area, which also incorporates O_3 and precursors recirculated the day before, as is shown in what follows.

Interesting results are also obtained by comparing the vertical profiles of BC and O_3 (Fig. 13). BC is a tracer of local primary pollution at ground level, and of the potential transport and stratification of regional/local primary pollutants (together or not with regional O_3) when present at high altitude. On 14 July 2015 07:06–08:21 UTC, at 350 m a.g.l. (and similarly for 15–17 July 2015 but at varying heights, 100–350 m a.g.l.) a clear discontinuity is evidenced with sudden and simultaneous decreases of BC and O_3 above these heights. The relatively high BC levels within the lower layer suggest nocturnal accumulation, while O_3 appears in strata

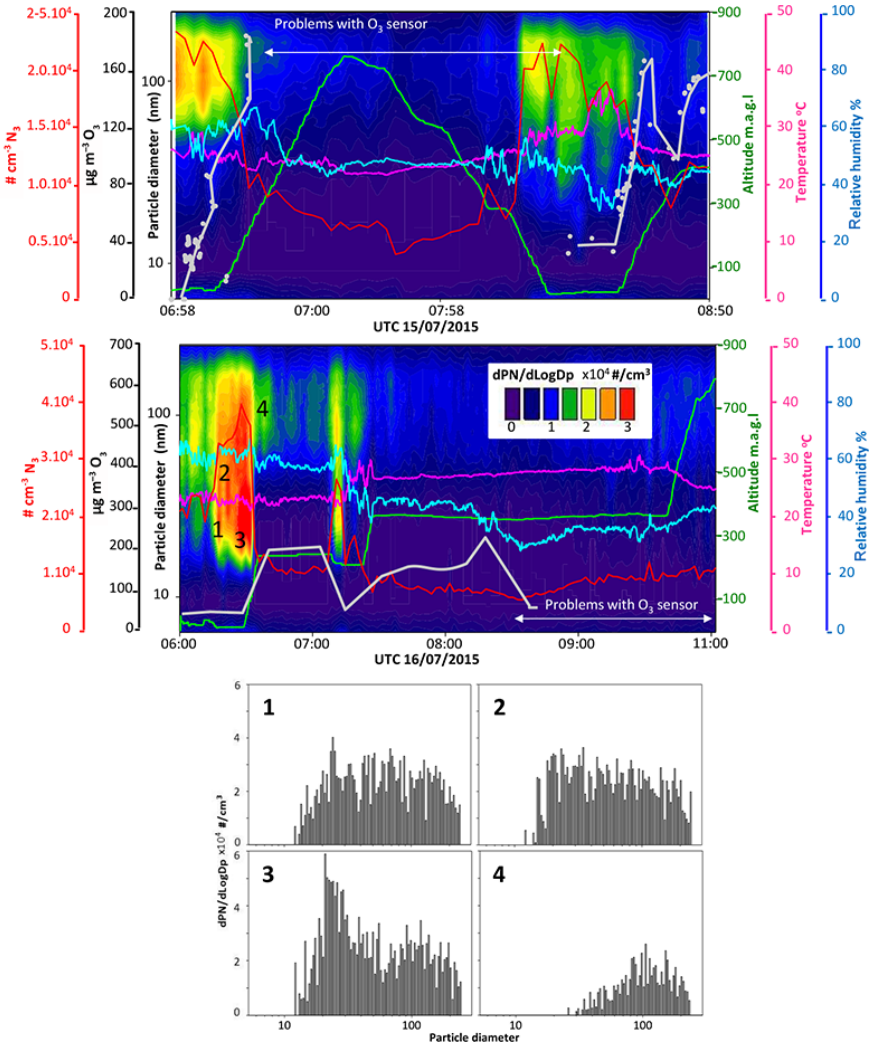

Figure 12. Time variation of altitude, temperature, relative humidity, N_3, particle number size distributions and O_3 concentrations during the tethered balloon measurements on 16 July 2015. 1–3 illustrate the nucleation episode recorded at surface level with particle number size distributions, and 4 the typical regional background N size distribution at about 300 m above ground.

(with low values near the ground due to titration and deposition) and with a high concentration just above that level (350 m), now with low BC concentrations. There is a further upward decrease of BC and an increase of O_3 up to the limit of the sounding (870 m).

The occurrence of an O_3 maximum layer around 100–200 m a.g.l., on top of the nocturnal stably stratified PBL, reinforces the idea of an important local production contributing to an upward increase of O_3 inside the layer. Finally, at the highest altitudes reached in this study (900–1000 m a.g.l.), BC and O_3 concentrations were often anti-correlated or unrelated, possibly more related with aged air masses recirculated within the whole region and with a mixed origin: including local-to-regional sources, more distant over the W-Mediterranean or even from hemispheric transport of air masses as reported by UNECE (2010).

Figure 14 shows mean O_3 hourly concentrations recorded at VIC for the episodes A and B, as well as mean wind speed and direction. Mean hourly concentrations are characterised by an increase until 10:00–11:00 UTC, followed by an inflexion point and a more marked increase, with a maximum between 13:00 and 14:00 UTC, and then a progressive decrease, more marked in episode A. As stated above, processes contributing to increased levels were attributable to fumigation, photochemical production and transport of high O_3 air masses, all controlled by insolation. Millán et al. (2000) described this characteristic diurnal O_3 pattern typically for inland valley stations (as in our case around 75 km from the coast), where the first O_3 increase is attributed to O_3 contributions from surface fumigation of high recirculated return strata as well as from the arrival of higher O_3 air masses transported by sea breeze and the local photochemi-

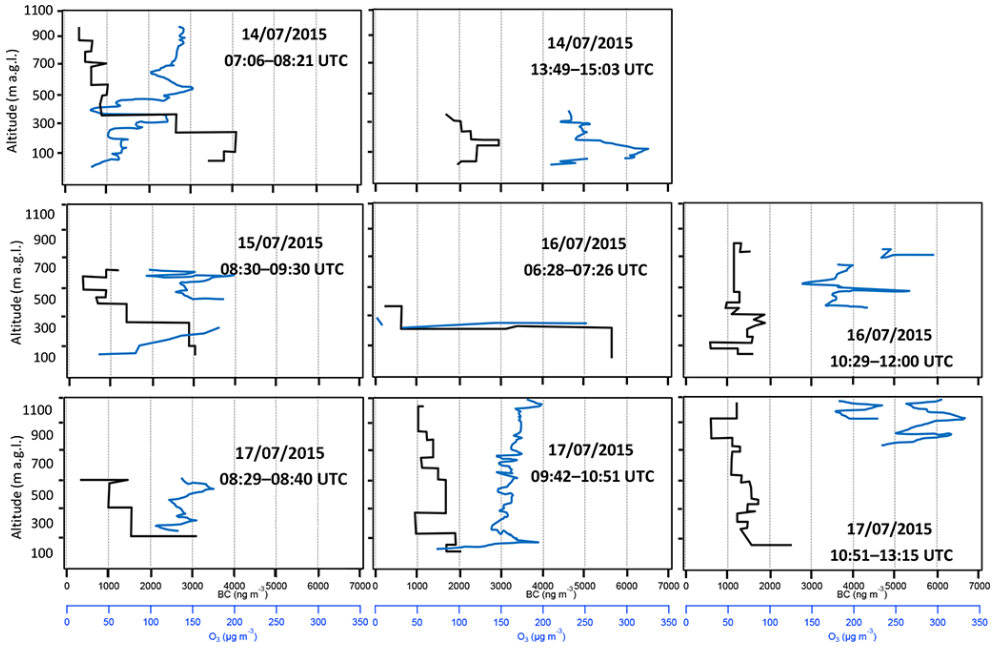

Figure 13. Vertical profiles of BC (5 min time resolution) and O_3 (10 s time resolution) at VIC.

cal production from precursors. On the other hand, the second O_3 concentration "hump" is coincident with maximum wind speed and probably corresponds to a more intensified sea-breeze transport compared with local photochemical formation and fumigation. Figure 14 shows that the two O_3 increases (and consequently the contributions from the three above processes) are more pronounced in the type A compared to the type B episode, and that the second maximum (more associated with inland surface transport by sea breeze) is wider, coinciding with a shift of the maximum wind speed towards the late afternoon, in the B episode.

Modelling outputs for the A episode point to light winds from the south, transporting pollutants from the BMA towards northern areas (including the Vic Plain), and triggering the hourly O_3 exceedances under the effect of the sea- and land-breeze transport. Thus, Figs. 15 and 16 show the horizontal wind vector at 10 m a.g.l. and NO_2 and O_3 concentrations both at ground level and at a height above the surface layer, at different hours for two representative days of the type A and B episodes, respectively. During the type A episode day (15 July 2015), the effect of the land-breeze transport accumulates NO_2 over the sea during the night, starting intense O_3 production when sun rises and sea breezes start the inland transport. Maximum concentrations of O_3, exceeding 180 µg m^{-3} were calculated by the model and measured at the stations located in the Vic Plain (TON, VIC and MAN, Fig. 16), although the model overestimated maximum O_3 concentrations in TON and VIC and delayed the hourly maximum value in all stations. The vertical distribution shows an important accumulation of around 110 µg m^{-3} trapped in a reservoir layer at around 1500 m a.s.l. during the

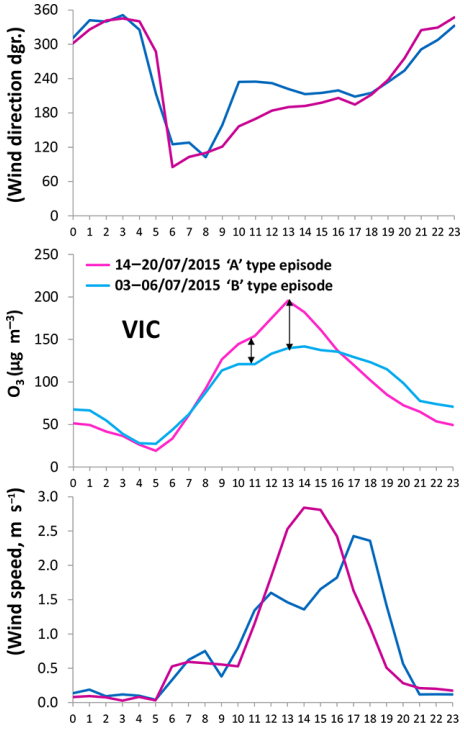

Figure 14. Mean hourly O_3 concentrations, and wind speed and wind direction for episodes A and B, showing higher levels in the A episodes for the two O_3 maxima.

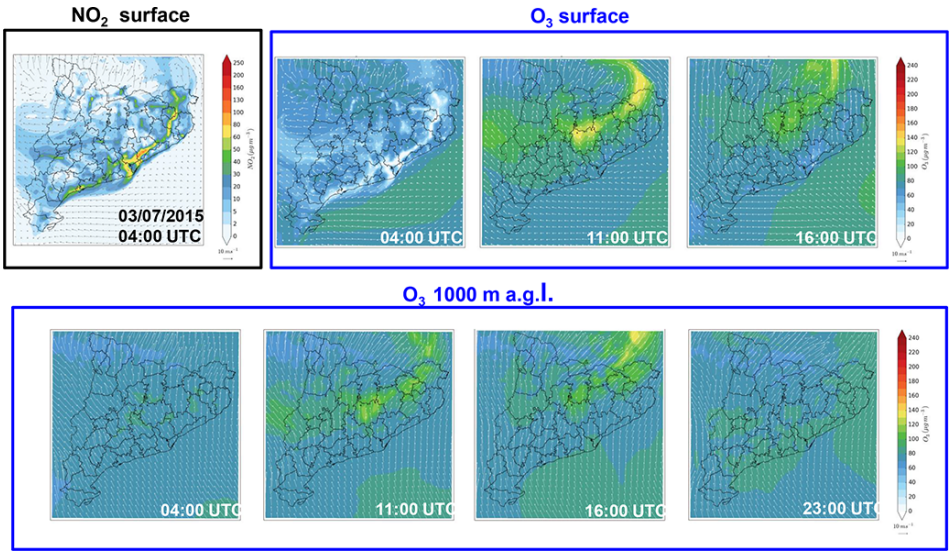

Figure 15. Maps of simulated NO_2 and O_3 concentrations at ground level with wind vectors at 10 m a.g.l. and at 1000 m a.g.l. with wind vectors at the same altitude, for selected hours on 3 July 2015.

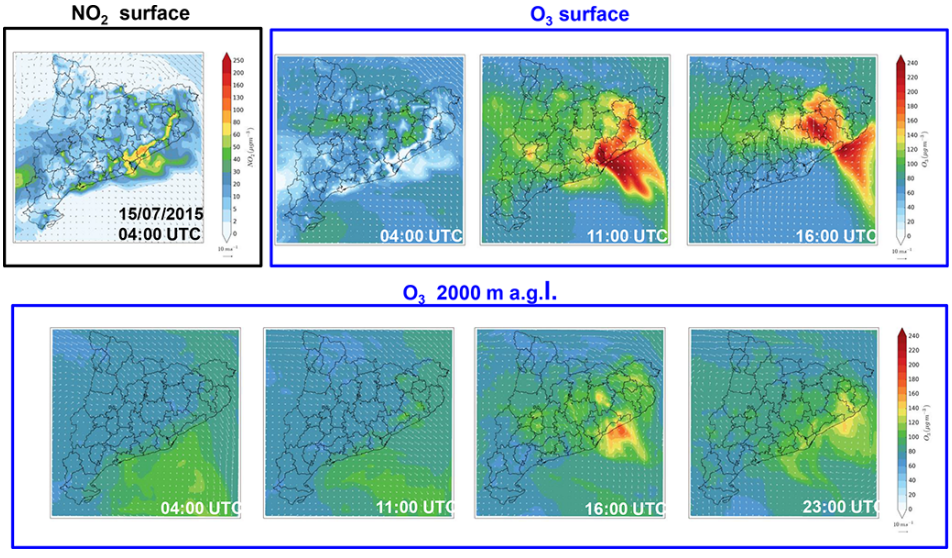

Figure 16. Maps of simulated NO_2 and O_3 concentrations at ground level with wind vectors at 10 m a.g.l. and at 2000 m a.g.l. with wind vectors at the same altitude, for selected hours on 15 July 2015.

night (Fig. 17), which will fumigate downwards into the new developing mixing layer during the following hours. Local O_3 production from fresh precursors accumulated during the night in the stably stratified surface layer and then progressed inland along the midday hours. This results in an O_3-enriched plume within a layer of 1000–1500 m depth in the late afternoon, following the model results (Fig. 17). This mixing layer also incorporates O_3 from upper reservoir layers after fumigation during the inland travel. The O_3 located at upper levels can recirculate back into the sea and will be potentially available to be transported inland (Millán et al., 1997, 2002), to start a new cycle the following day.

3.2.2 Type B episode (3–6 July 2015)

As opposed to the type A episode, during the type B episode and on 22–31 July 2015, despite the high O_3 and O_x concentrations, the concentrations were very similar in the urban and remote coastal sites and all along the northern sites, including the Vic Plain. Hence, the averaged O_x hourly concentrations of all the study sites were close to those at the coastal urban site in Barcelona CTL (and in the case of the O_3 close to the remote coastal site of BEG) compared with the large differences reported for the A episode (Fig. 8). The high O_x peak measured at the urban site during the mornings of

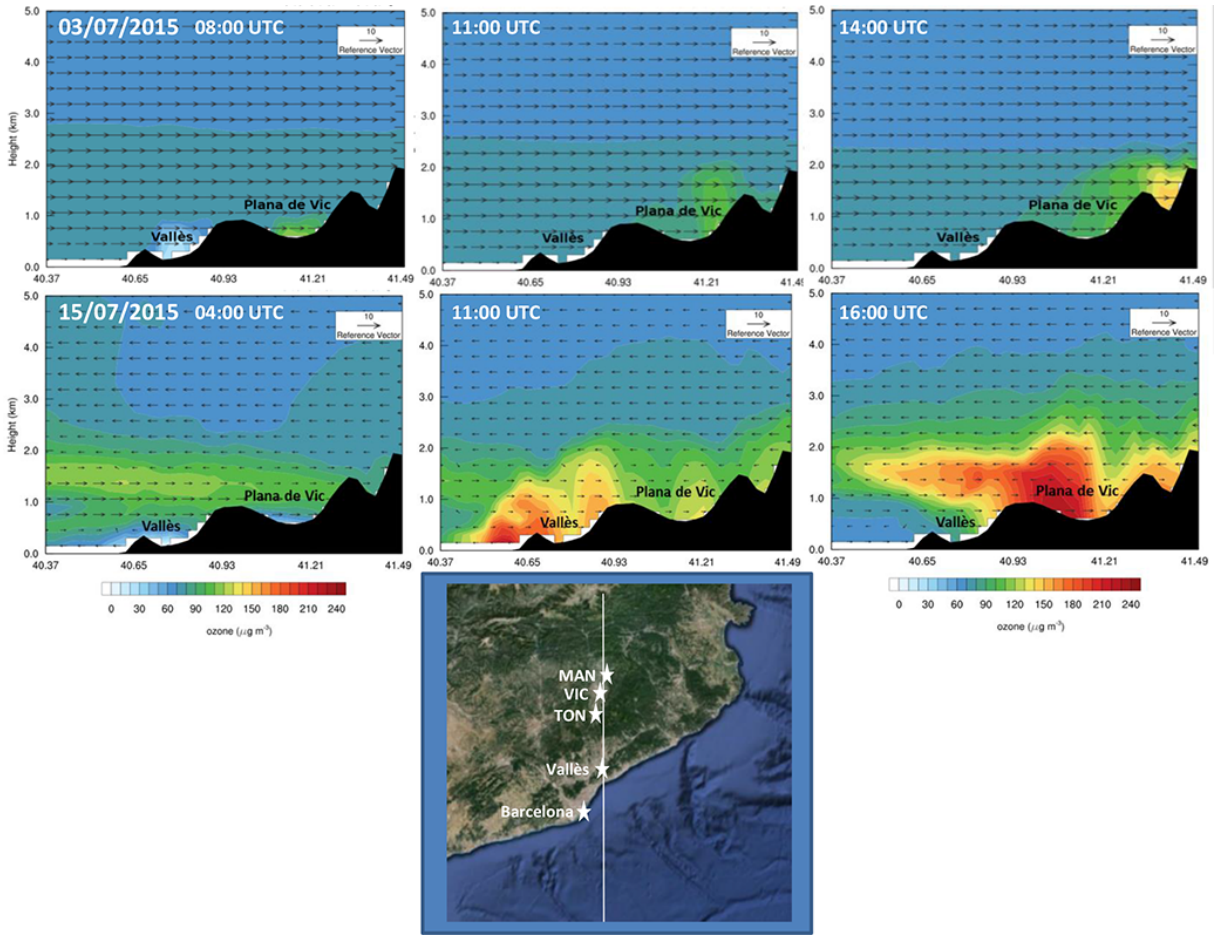

Figure 17. Spatial distributions of simulated O_3 concentrations and wind field vectors in the south–north vertical cross-section for different hours on 3 and 15 July 2015.

the B period (Fig. 8) and from 08:00 to 10:00 UTC in the average hourly patterns (Fig. 9) is probably due to the contribution of primary NO_2. According to Carslaw et al. (2016) the Euro 1 to Euro 2 diesel engines in Europe (early 1990s) emitted 5–10 % of primary NO_2 and 90–95 % of NO, whereas the Euro 4 to Euro 5 equivalent engines (2004 and 2009 onwards) emit 16–29 % of primary NO_2 and 71–84 % of NO.

Also as opposed to the A episode, during the B episode, O_x levels varied in a very narrow range from east (coastal) to west (mountains, MSC site) and from south (BMA) to north (Vic Plain) and at different heights (from Barcelona and BEG at sea level to MSC at 1570 m a.s.l.). Following the results of the model in Figs. 15 and 17, O_3 does not recirculate around the region in this period. There is no accumulation from one day to the next in reservoir layers located over the region. Southerly winds blow at height during the whole period and the combined sea-breeze and upslope winds developed at lower layers during daytime, after coupling with the southerlies, and vent out the O_3 production and the rest of the pollutants to the north. The circulation is open, as opposed to the type A episode, which show a closed circulation (it is never completely closed) (Millán et al., 1997, 2000). Unfortunately, vertical profiles of O_3, UFP, PM and BC profiles were not obtained for this episode.

Model outputs also evidence a net night and early morning transport of O_3 at lower layers from east and northeast during the B episode, supporting the hypothesis of a regional transport from southern France, advecting aged air masses to the whole region, while O_3 and its precursors from the BMA were transported during the morning to the southwest regions (Fig. 15) giving rise to hourly O_3 exceedances in some stations situated in this area. Figure 15 also shows that during this episode (3 July 2015) the combined sea breeze and upslope wind transported O_3 and precursors to the western pre-Pyrenees area, and values lower than 180 $\mu g\,m^{-3}$ were measured and modelled in all monitoring stations. The vertical distribution of O_3 also shows relatively low concentrations (as compared to 15 July) over most of the domain (Fig. 17).

4 Conclusions and implications for air quality

Very high levels of O_3 were recorded in the plains and valleys of the northern regions surrounding the BMA during July 2015, where 69 out of the 74 exceedances of the hourly O_3 information threshold measured in the entire air quality monitoring network of Catalonia were recorded. This represents a major environmental problem for which air quality managers must implement European and national legislation.

Both experimental measurements and modelling exercises suggest that these very intense O_3 episodes were originated by the concatenation of daily cycles of vertical recirculation of air masses that accumulated photochemically generated pollutants (Millán et al., 1997, 2000, 2002; Gangoiti et al., 2001; Castell et al., 2008a; Valverde et al., 2016), favoured by the high BVOCs and anthropogenic NO_x emissions in the BMA region. The lower 1000 m a.g.l. were highly enriched in O_3 by fumigation from precursors and O_3 located at upper levels (1500–3000 m a.g.l). Additionally, local contributions of O_3 to these episodes were also demonstrated by soundings of the lower layers (0–1000 m a.g.l.). Thus, slightly higher concentrations of O_3 were measured in stations located at the plains and inland valleys than at higher altitudes (up to 30–40 $\mu g\,m^{-3}$ exceeding the 180 $\mu g\,m^{-3}$ maximum hourly concentration reached in the mountain sites), due to the local photochemical production from fresh precursors emitted during the night and early morning, and their channelling within the combined upslope and sea-breeze circulation that transports O_3 and precursors from the BMA. Thus vertical profiles identified a high O_3 layer at 100–200 m a.g.l., produced by these local processes and also by the high deposition and titration of O_3 at the lower 100 m depth layer. In our (mostly rural) study low concentrations of UFPs were recorded at this high O_3 100–200 m a.g.l. layer and nucleation episodes were only detected into the PBL, most of the days at the lower atmospheric levels.

Two types of high O_3 episodes (A and B) were identified in the area:

Type A episodes are characterised by major local/regional O_3 recirculation, fumigation, production and transport, superimposed on the typical regional/long-range transport, and by the occurrence of major exceedances of the O_3 information threshold (14–20 July 2015). Surface fumigation from high O_3 return (to the sea) layers injected the day(s) before at altitudes of 1500–3000 m a.g.l., and recirculated over the VIC–TON–MAN area, as well as direct surface transport and formation of local/regional polluted air masses (with O_3 and precursors) from the BMA towards the north, decisively contributed to these exceedances. Thus, this atmospheric scenario is governed by poor ventilation under local breeze circulations and vertical recirculation of air masses over the study area.

Type B episodes are characterised by a major regional transport O_3 contribution, yielding similar O_x levels at all monitoring sites of the study area, with the arrival of aged air masses from the east/northeast (high O_3 levels entering through the coast), but without major transport from BMA to the Vic Plain (3–6 July 2015), and without vertical recirculation of air masses over the study area. When sunlight activated atmospheric photochemistry in the early morning, the northern regions were loaded with air masses with lower content of O_3 precursors, since air masses were transported from the BMA to the southwest (parallel to the coast) from 00:00 to 09:00 UTC. The combined breeze at midday favoured transport towards the northwest, rather than to the north, as described for the type A episode. In addition, the aged air masses are not vertically recirculated and leave the region towards the northeast (to France). Thus, O_3 concentrations were still relatively high (exceeding 120 $\mu g\,m^{-3}$ but below 180 $\mu g\,m^{-3}$) due to local production from fresh precursors and background O_3 contributions from the western Mediterranean, but not enough to exceed the information threshold.

From the perspective of possible precursor abatement strategies, direct mitigation measures at the BMA would have had a minor effect on O_3 concentrations at the Vic Plain area during the type B episode. However, during the type A episode, a reduction of NO_x and/or VOCs emissions in the BMA, some days before and during the episode, might have an effect on O_3 concentrations recorded in the Vic Plain. Nonetheless, due to the non-linearity of the O_3 generation processes, sensitivity analysis with high-resolution modelling is necessary to evaluate the possible effects in terms of absolute concentrations.

The use of O_x data from strategically selected monitoring sites in the east coast, western and central mountain areas, urban background sites of the BMA and sites in the Vic Plain, tracking the natural routes of pollutant transport, is a useful tool to assess the different regimes leading to high O_3 concentrations, and to differentiate between type A and type B episodes, with important implications in the design of potential abatement strategies.

We are aware that we only analysed the most intense O_3 episodes occurring in July 2015, and that there might be other scenarios, different to type A and B, yielding high O_3 events, such as the transport of aged air masses from other regions of Europe or the transport of the BMA emissions in meteorological scenarios different to those described here. However, in a recent study (Querol et al., 2016) we demonstrated with the analysis of the 2000–2015 O_3 data series that the Vic Plain (40–50 km north of Barcelona) is the area in Spain recording the highest number of annual exceedances of the O_3 information threshold, orders of magnitude higher than the surrounding areas of the axis BMA–Vic Plain–pre-Pyrenean ranges. Thus it is clear that the BMA emissions and the vertical recirculations caused by the local complex orography have an important role in the occurrence and development of intensive O_3 episodes in the region.

To implement potential (and difficult) abatement strategies two major key tasks are proposed:

1. Meteorological forecasting from June to August to predict recirculation episodes in order to apply abatement measures for O_3 precursors before a recirculation episode starts. As stated above, the relevance of these recirculations in originating these high O_3 episodes in southern Europe has been assumed already by the European Commission (EC, 2004).

2. Sensitivity analysis with high-resolution modelling to evaluate the effectiveness of NO_x and VOCs abatement measures on O_3 reduction.

5 Data availability

Hourly measurements of gaseous pollutants at the 48 monitoring sites belonging to the regional air quality network used in this paper can be downloaded from the regional air quality monitoring network (XVPCA) at http://dtes.gencat.cat/icqa. Table S1 in the Supplement gives details of these monitoring sites.

The meteorological data from the stations used can be requested free of charge from smc@meteo.cat. Table S3 in the Supplement gives details of these monitoring sites.

In an Excel file included in the Supplement, data from diffusion tubes for NO_2 and O_3 are reported. Finally, data from measurements with tethered balloons can be requested by mail from the corresponding authors of this paper.

The Supplement related to this article is available online at doi:10.5194/acp-17-2817-2017-supplement.

Competing interests. The authors declare that they have no conflict of interest.

Acknowledgements. The present work was supported by the Spanish Ministry of Economy and Competitiveness and FEDER funds under the project HOUSE (CGL2016-78594-R), by the Generalitat de Catalunya (AGAUR 2015 SGR33 and the DGQA). Part of this research was supported by the Korean Ministry of the Environment through "The Eco-Innovation project". The participation of University of Marseille and University of Birmingham was partially supported by two TNA actions projects carried out under the ACTRIS2 project (grant agreement No. 654109) financed by the European Union's Horizon 2020 research and innovation program. The support of the CUD of Zaragoza (project CUD 2013-18) is also acknowledged. We are very thankful to the Generalitat de Catalunya for supplying the air quality data from the XVPCA stations, to METEOCAT (the Meteorological Office of Catalonia) for providing meteorological data and to the IES J. Callís and the Meteorological Station from Vica (especially to Manel Dot) for allowing the performance of the vertical profiles and mobile unit measurements, respectively. In memoriam of Andrei Lyasota.

Edited by: F. Dentener
Reviewed by: two anonymous referees

References

Ajuntament de Barcelona: Annual Statistics of the Barcelona City, available at: http://www.bcn.cat/estadistica/catala/dades/anuari/cap15/index.htm (last access: 7 September 2016), 2015.

Barros, N., Borrego, C., Toll, I., Soriano, C., Jiménez, P., and Baldasano, J. M.: Urban Photochemical Pollution in the Iberian Peninsula: Lisbon and Barcelona Airsheds, J. Air Waste Manage., 53, 347–359, 2003.

Byun, D. W. and Ching, J. K. S.: Science algorithms of the EPA Models-3 Community Multiscale Air Quality (CMAQ) modeling system, National Exposure Research Laboratory, US Environmental Protection Agency, Research Triangle Park, NC: Atmospheric Modelling Division, 27711, 1999.

Carslaw, D. C.: The openair manual – open-source tools for analysing air pollution data, Manual for version 0.7-0, King's College, London, 2012.

Carslaw, D. C., Murrells, T. P., Andersson, J., and Keenan, M.: Have vehicle emissions of primary NO_2 peaked?, Faraday Discuss., 189, 439–454, 2016.

Castell, N., Mantilla, E., and Millán, M. M.: Analysis of tropospheric ozone concentration on a Western Mediterranean site: Castellon (Spain), Environ. Monit. Assess., 136, 3–11, 2008a.

Castell, N., Stein, A. F., Salvador, R., Mantilla, E., and Millán, M. M.: The impact of biogenic VOC emissions on photochemical ozone formation during a high ozone pollution episode in the Iberian Peninsula in the 2003 summer season, Adv. Sci. Res., 2, 9–15, 2008b.

Castell, N., Tellez, L., and Mantilla, E.: Daily, seasonal and monthly variations in ozone levels recorded at the Turia river basin in Valencia (Eastern Spain), Environ. Sci. Pollut. R., 19, 3461–3480, 2012.

Cusack, M., Pérez, N., Pey, J., Alastuey, A., and Querol, X.: Source apportionment of fine PM and sub-micron particle number concentrations at a regional background site in the western Mediterranean: a 2.5 year study, Atmos. Chem. Phys., 13, 5173–5187, doi:10.5194/acp-13-5173-2013, 2013.

DGT: Dirección General de Tráfico: Anuario Estadístico General, available at: http://www.dgt.es/es/seguridad-vial/estadisticas-e-indicadores/publicaciones/anuario-estadistico-general/ (last access: 6 December 2015), 2014.

Dieguez, J. J., Millán, M., Padilla, L., and Palau, J. L.: Estudio y evaluación de la contaminación atmosférica por ozono troposférico en España, CEAM Report for the Ministry of Agriculture, Food and Environment, INF FIN/O3/2009, 372 pp., available at: http://origin.magrama.gob.es/es/calidad-y-evaluacion-ambiental/temas/atmosfera-y-calidad-del-aire/8_A_Informe_final_ozono-ceam_Julio_2009_tcm7-438818.pdf (last access: 14 February 2017), 2009.

Dieguez, J. J., Calatayud, V., and Mantilla, E.: CEAM Report for the Ministry of Agriculture, Food and Environment, Fundación Biodiversidad, Informe Final, Memoria Técnica Proyecto CONOZE, CONtaminación por OZono en España, 137 pp., available at:

http://www.mapama.gob.es/es/calidad-y-evaluacion-ambiental/temas/atmosfera-y-calidad-del-aire/Informe_t%C3%A9cnico_CONOZE[1]_tcm7-330956.pdf (last access: 14 February 2017), 2014.

Doherty, R. M., Wild, O., Shindell, D. T., Zeng, G., Collins, W. J., MacKenzie, I. A., Fiore, A. M., Stevenson, D. S. Dentener, F. J., Schultz, M. G., Hess, P., Derwent, R. G., and Keating, T. J.: Impacts of climate change on surface ozone and intercontinental ozone pollution: A multi-model study, J. Geophys. Res., 118, 3744–3763, 2013.

Doval, M., Castell, N., Téllez, L., and Mantilla, E.: The use of experimental data and their uncertainty for assessing ozone photochemistry in the Eastern Iberian Peninsula, Chemosphere, 89, 796–804, 2012.

EC: European Commission Decision of 19 March 2004, Concerning guidance for implementation of Directive 2002/3/EC of the European Parliament and the Council relating to ozone in ambient air (2004/279/EC), Official Journal of the European Union L87/50, 2004.

EEA: Air quality in Europe-2015 report, EEA Report, No 5/2015, ISSN 1977-8449, 2015.

Escudero, M., Lozano, A., Hierro, J., del Valle, J., and Mantilla, E.: Urban influence on increasing ozone concentrations in a characteristic Mediterranean agglomeration, Atmos. Environ., 99, 322–332, 2014.

Gangoiti, G., Millán, M. M., Salvador, R., and Mantilla, E.: Long-range transport and re-circulation of pollutants in the western Mediterranean during the project Regional Cycles of Air Pollution in the West-Central Mediterranean Area, Atmos. Environ., 35, 6267–6276, 2001.

Gangoiti, G., Alonso, L., Navazo, M., García, J. A., and Millán, M. M.: North African soil dust and European pollution transport to America during the warm season: Hidden links shown by a passive tracer simulation, J. Geophys. Res., 111, D10109, doi:10.1029/2005JD005941, 2006.

Geiger, R., Aron, R. H., and Todhunter P.: The Climate Near the Ground. Rowman & Littelefield Publishers Inc., 6th Edn., ISBN 0-7425-1857-4, Lonham, US, 561 pp., 1992.

Gonçalves, M., Jiménez-Guerrero, P., and Baldasano, J. M.: Contribution of atmospheric processes affecting the dynamics of air pollution in South-Western Europe during a typical summertime photochemical episode, Atmos. Chem. Phys., 9, 849–864, doi:10.5194/acp-9-849-2009, 2009.

Hertel, O., Skjøth, C. A., Reis, S., Bleeker, A., Harrison, R. M., Cape, J. N., Fowler, D., Skiba, U., Simpson, D., Jickells, T., Kulmala, M., Gyldenkærne, S., Sørensen, L. L., Erisman, J. W., and Sutton, M. A.: Governing processes for reactive nitrogen compounds in the European atmosphere, Biogeosciences, 9, 4921–4954, doi:10.5194/bg-9-4921-2012, 2012.

Hewson, E. W.: Industrial Air Pollution Meteorology, Meteorological Laboratories of the College of Engineering, The University of Michigan, Ann Arbor, MI, 191 pp., 1964.

Kley, D. and Geiss, H.: Tropospheric ozone at elevated sites and precursor emissions in the United States and Europe, Atmos. Environ., 8, 149–158, 1994.

Lee, H.-K., Hwang, I.-K., and Ahn, K.-H.: Development and Evaluation of Hy-CPC, Particle and Aerosol Research, 10, 93–97, 2014.

Lee, H.-K., Eun, H.-R., Lee, G.-H., and Ahn, K.-H.: Development and evaluation of Hy-SMPS, Particle and Aerosol Research, 11, 57–61, 2015.

Mantilla, E., Millán, M. M., Sanz, M. J., Salvador, R., and Carratalá, A.: Influence of mesometeorological processes on the evolution of ozone levels registered in the Valencian Community, in: I Technical workshop on ozone pollution in southern Europe, Valencia, 1997.

Millán, M. M. (Ed.): Ozone Dynamics in the Mediterranean Basin: A collection of scientific papers resulting from the MECAPIP, RECAPMA and SECAP Projects, European Commission (DG RTD I.2) Air Pollution Research Report 78, available from CEAM, Valencia, Spain, 287 pp., 2002.

Millán, M. M.: Extreme hydrometeorological events and climate change predictions in Europe, J. Hydrol., 518, 206–224, 2014.

Millán, M. M. and Sanz, M. J.: Ozone in Mountainous regions and in Southern Europe, in: Ad hoc Working group on Ozone Directive and Reduction Strategy Development, Ozone Position Paper, 145–150, European Commission, Brussels, 1999.

Millán, M. M., Artiñano, B., Alonso, L., Navazo, M., and Castro, M.: The effect of meso-scale flows on regional and long-range atmospheric transport in the Western Mediterranean area, Atmos. Environ., 25, 949–963, 1991.

Millán, M. M., Salvador, R., Mantilla, E., and Artiñano, B.: Meteorology and photochemical air pollution in southern Europe: experimental results from EC research projects, Atmos. Environ., 30, 1909–1924, 1996a.

Millán, M. M., Mantilla, E., Salvador, R., and Kallos, G.: Regional and long-range transport scenarios for photo-oxidants on the Mediterranean basin in summer, Ninth joint conference on applications of air pollution meteorology, 438–441, American Meteorological Society, Boston, 1996b.

Millán, M. M., Salvador, R., and Mantilla, E.: Mesoscale processes and photo-oxidants cycles on the Spanish Mediterranean coast, Ninth joint conference on applications of air pollution meteorology, 434–437, American Meteorological Society, Boston, 1996c.

Millán, M. M., Salvador, R., Mantilla, E., and Kallos, G.: Photooxidant dynamics in the Mediterranean basin in summer: Results from European research projects, J. Geophys. Res., 102, 8811–8823, 1997.

Millán, M. M., Mantilla, E., Salvador, R., Carratalá, A., Sanz, M. J., Alonso, L., Gangoiti, G., and Navazo, M.: Ozone Cycles in the Western Mediterranean Basin: Interpretation of Monitoring Data in Complex Coastal Terrain, J. Appl. Meteorol., 39, 487–508, 2000.

Millán, M. M., Sanz, M. J., Salvador, R., and Mantilla, E.: Atmospheric dynamics and ozone cycles related to nitrogen deposition in the western Mediterranean, Environ. Pollut., 118, 167–186, 2002.

Minguillón, M. C., Brines, M., Pérez, N., Reche, C., Pandolfi, M., Fonseca, A. S., Amato, F., Alastuey, A., Lyasota, A., Codina, B., Lee, H.-K., Eun, H.-R., Ahn, K.-H., and Querol, X.: New particle formation at ground level and in the vertical column over the Barcelona area, Atmos. Res., 164–165, 118–130, 2015.

Monks, P. S., Archibald, A. T., Colette, A., Cooper, O., Coyle, M., Derwent, R., Fowler, D., Granier, C., Law, K. S., Mills, G. E., Stevenson, D. S., Tarasova, O., Thouret, V., von Schneidemesser, E., Sommariva, R., Wild, O., and Williams, M. L.: Tropospheric ozone and its precursors from the urban to the global scale from

air quality to short-lived climate forcer, Atmos. Chem. Phys., 15, 8889–8973, doi:10.5194/acp-15-8889-2015, 2015.

Palacios, M., Kirchner, F., Martilli, A., Clappier, A., Martín, F., and Rodríguez, M. E.: Summer ozone episodes in the Greater Madrid area. Analyzing the ozone response to abatement strategies by modelling, Atmos. Environ., 36, 5323–5333, 2002.

Pay, M. T., Valverde, V., Baldasano, J. M., Kwok, R., Napelenok, S., and Baker, K.: PhotochemicalModeling to Attributing Source and Source Regions to Ozone Exceedances in Spain, 13th Annual CMAS Conference, Chapel Hill, NC, October 27–29, available at: https://www.cmascenter.org/conference/2014/slides/maria_pay_photochemical_modeling_2014.pptx (last access: 14 February 2017), 2014.

Querol, X., Alastuey, A., Rodríguez, S., Plana, F., Ruiz, C. R., Cots, N., Massagué, G., and Puig, O.: PM_{10} and $PM_{2.5}$ source apportionment in the Barcelona Metropolitan Area, Catalonia, Spain, Atmos. Environ., 35/36, 6407–6419, 2001.

Querol, X., Alastuey, A., Orio, A., Pallares, M., Reina, F., Dieguez, J. J., Mantilla, E., Escudero, M., Alonso, L., Gangoiti, G., and Millán, M.: On the origin of the highest ozone episodes in Spain, Sci. Total Environ., 572, 379-389, 2016.

Rodríguez, S., Querol, X., Alastuey, A., and Mantilla, E.: Origin of high summer PM_{10} and TSP concentrations at rural sites in Eastern Spain, Atmos. Environ., 36, 3101–3112, 2002.

Salvador, R., Millán, M. M., Mantilla, E., and Baldasano, J. M.: Mesoscale modelling of atmospheric processes over the western Mediterranean area during summer, Int. J. Environ. Poll., 8, 513–528, 1997.

Salvador, R., Millán, M. M., and Calbo, J.: Horizontal Grid Size Selection and its influence on Mesoscale Model Simulations, J. Appl. Meteorol., 38, 1311–1329, 1999.

Seco, R., Peñuelas, J., Filella, I., Llusià, J., Molowny-Horas, R., Schallhart, S., Metzger, A., Müller, M., and Hansel, A.: Contrasting winter and summer VOC mixing ratios at a forest site in the Western Mediterranean Basin: the effect of local biogenic emissions, Atmos. Chem. Phys., 11, 13161–13179, doi:10.5194/acp-11-13161-2011, 2011.

Skamarock, W. C., Klemp, J. B., Gill, D. O., Barker, D. M., and Powers, J. G.: A description of the advanced research WRF version 3, NCAR. Tech. Note NCAR/TN-468+STR, 88 pp., NCAR, Boulder, Colorado, USA, 2008.

Soler, M. R., Hinojosa, J., Bravo, M., Pino, D., and Vilà Guerau de Arellano, J.: Analyzing the basic features of different complex terrain flows by means a Doppler Sodar and a numerical model: Some implications to air pollution problems, Meteorol. Atmos. Phys., 1–3, 141–154, 2004.

Soler, M. R., Arasa, A., Merino, M., Olid, M., and Ortega, S.: High vertical resolution numerical simulation of the sea-breeze flow in Catalonia. Implications to spatial and temporal variability of ozone and PM_{10} levels, Bound.-Lay. Meteorol., 140, 37–56, 2011.

Soler, R. M., Gámez, P., and Olid, M.: Aramis a regional air quality model for air pollution management: evaluation and validation, Física de la Tierra, 27, 111–136, 2015.

Stein, A. F., Mantilla, E., and Millán, M. M.: Ozone formation downwind an industrial complex in the western Mediterranean, in: 13th World Clean Air and Environmental Protection, 22–27 August, London, UK, 2004.

Stein, A. F., Mantilla, E., and Millán, M. M.: Using measured and modelled indicators to assess ozone-NO_x-VOC sensitivity in a western Mediterranean coastal environment, Atmos. Environ., 39, 7167–7180, 2005.

Tang, Y. S., Cape, J. N., and Sutton, M. A.: Development and types of passive samplers for NH_3 and NO_x, in: Proceedings of the International Symposium on Passive Sampling of Gaseous Pollutants in Ecological Research, Science World, Vol. 1, 513–529, 2001.

Toll, I. and Baldasano, J. M.: Modeling of photochemical air pollution in the Barcelona area with highly disaggregated anthropogenic and biogenic emissions, Atmos. Environ., 34, 3069–3084, 2000.

UNECE: Hemispheric transport of air pollution 2010, Part A: ozone and particulate matter, Air pollution studies, 17. UNECE, LRTAP, Task Force on Hemispheric Transport of Pollutants HTAP 2010: Part A. Ozone and Particulate Matter, 278 pp., ECE/EB.AIR/100, available at: http://www.htap.org/publications/2010_report/2010_Final_Report/HTAP2010PartA110407.pdf (last access: 14 February 2017), 2010.

Valverde, V., Pay, M. T., and Baldasano, J. M.: Ozone attributed to Madrid and Barcelona on-road transport emissions: Characterization of plume dynamics over the Iberian Peninsula, Sci. Total Environ., 543, 670–682, 2016.